①

AD-A181 567

Technical Report C87-02
April 1987

TECHNICAL REPORT FOR THE PERIOD
1 JANUARY – 31 MARCH 1987

DTIC
ELECTE
JUN 1 0 1987
S   D
C&D

Center Staff

SPONSORED BY:

DEFENSE ADVANCED RESEARCH PROJECTS AGENCY

87   6 ○   0 2 2

Technical Report C87–02
April 1987

TECHNICAL REPORT FOR THE PERIOD
1 JANUARY — 31 MARCH 1987

Center Staff

REPORT DOCUMENTATION PAGE

AD-A181 567

1a. REPORT SECURITY CLASSIFICATION
Unclassified

2a SECURITY CLASSIFICATION AUTHORITY	3 DISTRIBUTION/AVAILABILITY OF REPORT
2b DECLASSIFICATION/DOWNGRADING SCHEDULE	Unlimited

4 PERFORMING ORGANIZATION REPORT NUMBER(S)	5. MONITORING ORGANIZATION REPORT NUMBER(S)
SAIC-87/1062 Technical Report C87-02	

6a NAME OF PERFORMING ORGANIZATION Science Applications International Corporation	6b OFFICE SYMBOL (If applicable)	7a. NAME OF MONITORING ORGANIZATION Defense Supply Service – Washington

6c. ADDRESS (City, State, and ZIP Code) Center for Seismic Studies/SAIC 1300 N. 17th Street, Suite 1450 Arlington, Virginia 22209-3871	7b. ADDRESS (City, State, and ZIP Code) Room 1D245, The Pentagon Washington, D.C. 20310

8a. NAME OF FUNDING/SPONSORING ORGANIZATION Defense Advanced Research Projects Agency	8b OFFICE SYMBOL (If applicable) STO/GSD	9. PROCUREMENT INSTRUMENT IDENTIFICATION NUMBER MDA-84-C-0020

8c. ADDRESS (City, State, and ZIP Code) 1400 Wilson Boulevard Arlington, Virginia 22209	10. SOURCE OF FUNDING NUMBERS			
	PROGRAM ELEMENT NO.	PROJECT NO.	TASK NO.	WORK UNIT ACCESSION NO
		A04882		

11. TITLE (Include Security Classification)

Technical Report for the Period 1 January – 31 March 1987   (Unclassified)

12. PERSONAL AUTHOR(S) R. Baumstark, G. Bulin, A. Campanella, P. Dysart, H. Israelsson, A. Jurkevics, J. Pulli, M. Tiberio, C. Romney, A. Ryall

13a. TYPE OF REPORT Technical Report	13b. TIME COVERED FROM 1/1 TO 3/31/87	14. DATE OF REPORT (Year, Month, Day) 1987 April	15 PAGE COUNT 75

16. SUPPLEMENTARY NOTATION

17.	COSATI CODES		18. SUBJECT TERMS (Continue on reverse if necessary and identify by block number)
FIELD	GROUP	SUB-GROUP	Seismology Attenuation Nuclear Monitoring GSE Seismic Networks Regional Propagation

19 ABSTRACT (Continue on reverse if necessary and identify by block number)

Work continued during this reporting period on the assessment of capabilities of seismic networks and the design of networks to achieve specified performance characteristics. Results included in this report show that a network's location accuracy approaches a near-maximum when stations are distributed over an azimuthal sector of about 180 degrees and that good depth determination requires stations within about 15 degrees of the focus of the event. The latter suggests that global networks should include 100 or more stations if accurate depth estimation is important. As in previous reports, this work continues to be directed toward networks of the type being considered by the Group of Scientific Experts (GSE).

(*Continued on attached sheet*)

20 DISTRIBUTION/AVAILABILITY OF ABSTRACT ☒ UNCLASSIFIED/UNLIMITED ☐ SAME AS RPT. ☐ DTIC USERS	21. ABSTRACT SECURITY CLASSIFICATION Unclassified
22a. NAME OF RESPONSIBLE INDIVIDUAL Ann U. Kerr	22b. TELEPHONE (Include Area Code) (202) 694-3624	22c OFFICE SYMBOL STO/GSD

DD FORM 1473, 84 MAR   83 APR edition may be used until exhausted
 All other editions are obsolete

19. Abstract - (*Continued*)

An interim report is included on a study of about 100 local and regional events detected by NORESS. This study is a systematic effort to test analytical methods being developed at the Center for extracting features from seismic waveforms that can be used to identify regional phases, and for recognizing repeated events from a single source such as quarry blasts. The methods under evaluation include the extraction of frequency-domain spectral parameters, time-domain spectral paramenters, and particle motion information. This work has particular application to analysis of three-component data at GSE "National Data Centers." However, the work on recognizing repeated sources is also applicable to array stations, and the phase identification work is also applicable to identifying phases not separable by conventional f-k analysis from array data (e.g., *Sn* vs. *Lg*).

Substantial effort during this quarter was devoted to developing concepts and preparing for experiments in international exchange of seismic waveform data. This work included developing the technical concepts for a potential global seismic monitoring system, (with much interaction with DARPA) and preparing the report (GSE/US/44) that was subsequently tabled in Geneva at the GSE meeting in March. Other GSE work included installing and debugging the "automatic association" program on the Center's GSE Sun computer (in lieu of a VAX), and providing the program to Australia for the data center being developed there for GSE experiments. Waveform exchange experiments, initiated during 1986 with the exchange of a few waveforms, became an important activity during this quarter as described in this report.

Our investigation of the sensitivity of m_b to changes in t^* have now been extended to explosions at twelve sites. This work continues to show that m_b is least affected by Δt^* if Q is frequency dependent, and that the m_b correction for Δt^* is a function of magnitude itself (as expected from theory). An apparent dependence of magnitude anomalies on explosion magnitude has been noted for Soviet tests recorded at NORESS. Capabilities of three-component stations to determine teleseismic source-direction by polarization analysis are nearing completion, and show that a useful analytical tool for GSE National Data Centers is available.

The Center has been heavily involved in an examination of its database management system and the development of extensions to handle new types of data--principally data from seismic arrays and data anticipated from forthcoming GSE experiments. Working jointly with Science Horizons, Inc., and SAIC's La Jolla-based geophysics group, the Center plans to propose a revision of its version 2.7 database structure during the next quarter. Major work on building databases containing NORESS data has continued, and progress reports on this and other database development are included.

Table of Contents

Availability Codes

Dist | Avail and/or Special

A-1

1. FOREWORD

Work continued during this reporting period on the assessment of capabilities of seismic networks and the design of networks to achieve specified performance characteristics. Results reported in Section 2 show that a network's location accuracy approaches a near-maximum when stations are distributed over an azimuthal sector of about 180 degrees and that good depth determination requires stations within about 15 degrees of the focus of the event. The latter suggests that global networks should include 100 or more stations if accurate depth estimation is important. As in previous reports, this work continues to be directed toward networks of the type being considered by the Group of Scientific Experts (GSE).

Section 3 presents an interim report on a study of about 100 local and regional events detected by NORESS. This study is a systematic effort to test analytical methods being developed at the Center for extracting features from seismic waveforms that can be used to identify regional phases, and for recognizing repeated events from a single source such as quarry blasts. The methods under evaluation include the extraction of frequency-domain spectral parameters, time-domain spectral paramenters, and particle motion information. This work has particular application to analysis of three-component data at GSE "National Data Centers." However, the work on recognizing repeated sources is also applicable to array stations, and the phase identification work is also applicable to identifying phases not separable by conventional f-k analysis from array data (e.g., Sn vs. Lg).

Substantial effort during this quarter was devoted to developing concepts and preparing for experiments in international exchange of seismic waveform data. This work included developing the technical concepts for a potential global seismic monitoring system (with much interaction with DARPA) and preparing the report (GSE/US/44) that was subsequently tabled in Geneva at the GSE meeting in March. Other GSE work included installing and debugging the "automatic association" program on the Center's GSE Sun computer (in lieu of a VAX), and providing the program to Australia for the data center being developed there for GSE experiments. Waveform exchange experiments, initiated during 1986 with the exchange of a few waveforms, became an important activity during this quarter; details are given in Section 4 of this report.

Progress reports on a number of other activities at the Center are given in Section 5. Our investigation of the sensitivity of m_b to changes in t^* have now been extended to explosions at twelve sites. This work continues to show that m_b is least affected by Δt^* if Q is frequency dependent, and that the m_b correction for Δt^* is a function of magnitude itself (as expected from theory). An apparent dependence of magnitude anomalies on explosion magnitude has been noted for Soviet tests recorded at NORESS. Capabilities of three-component stations to determine teleseismic source-direction by polarization analysis are nearing completion, and show that a useful analytical tool for GSE National Data Centers is available.

The Center has been heavily involved in an examination of its database management system and the development of extensions to handle new types of data—principally data from seismic arrays and data anticipated from forthcoming GSE experiments. Working jointly with Science Horizons, Inc., and SAIC's La Jolla-based geophysics group, the Center plans to propose a revision of its version 2.7 database structure during the next quarter. Major work on building databases containing NORESS data has continued, and progress reports on this and other database development is also contained in Section 5.

2. NETWORK CAPABILITY AND DESIGN

2.1. A NOTE ON NETWORK DESIGN: STATION DISTRIBUTION AND EPICENTER ERROR

2.1.1. Introduction

Determination of the epicenter of a detected seismic event is one important function for seismological test ban monitoring. For example, a precise epicenter determination is important for an event the nature of which can not readily be established. This is the case particularly if it occurs close to territorial boundaries or if such an event is selected for on-site inspection.

The quality of an epicenter estimate depends on several factors one of which is the geometry of the detecting stations in relation to the epicenter. A symmetrical distribution of the stations around the azimuth from the event is often considered desirable. This is, however, often not possible to achieve in practice. In this note we attempt to describe how uncertainties in epicenter determination vary with the relative location of the detecting seismic stations. The analysis is illustrated with calculated location errors for hypothetical station networks.

2.1.2. Model

Estimation of the epicenter (latitude and longitude) of an event is part of the seismic event location procedure, which also simultaneously gives estimates of origin time and focal depth. In this note the analysis is, however, limited to the joint marginal confidence region for the estimated epicenter (Flinn, 1965).

We introduce a Cartesian coordinate system, $\mathbf{X}=(x_1,x_2)$, with origin at the true epicenter. The epicenter determination is assumed to be based on first-arrival time readings at n stations, which are located at distances Δ_k and azimuths ϕ_k from the epicenter. The arrival time residuals or data errors are assumed to be normally distributed and are characterized by an *a priori* standard deviation, σ. These data errors include reading errors at the stations as well as uncertainties of the travel time model. Since standard error is usually dominated by uncertainties in the travel time model, it is assumed here that all observations have the same σ.

The joint marginal confidence region for the estimated epicenter is given by

$$\sigma^{-2}\cdot\mathbf{X}^T\cdot\mathbf{S}\cdot\mathbf{X}\leqslant\chi_2^p(2)$$

The elements of the symmetrical covariance matrix S are determined by the relative locations of the n detecting stations as described by their azimuths from the source ($\phi_k; k=1,2,...,n$) and their slowness values ($\dfrac{dT}{d\Delta_k}$):

$$S_{11}=\sum\left(\frac{dT}{d\Delta_k}\right)^2 \cdot \cos^2(\phi_k)$$

$$S_{22}=\sum\left(\frac{dT}{d\Delta_k}\right)^2 \cdot \sin^2(\phi_k)$$

$$S_{12}=\sum\left(\frac{dT}{d\Delta_k}\right)^2 \cdot \cos(\phi_k)\cdot\sin(\phi_k)$$

In order to simplify the expressions above for the elements of the matrix S is assumed that the epicenter of the event is located at the north pole. The confidence region is an ellipse and the orientation and lengths of the axes (a and b) are thus determined by the elements of the matrix S.

We will use the area (i.e., $\pi \cdot a \cdot b$) and the square root of the area of this confidence ellipse as measures of the location error. Since we consider location errors in contexts like on-site inspection, the area is used rather than the major axis as a measure of the location error.

It can be shown that the area of the confidence ellipse is inversely proportional to the determinant of the matrix S:

$$\pi \cdot a \cdot b = \pi \chi_{2_p}(2) \cdot \sigma^2 / (S_{11} \cdot S_{22} - S_{12}^2)$$

This formula is 180 degrees symmetric with regard to the azimuthal station distribution. In other words if a station is moved 180 degrees around the source azimuth the location error will still be the same. This means that a 360 degree coverage of stations around the source azimuth will not give a smaller location error than a coverage of 180 degrees. This conclusion is based on the particular assumptions about the model used here; in practice, due to lateral variation of the velocity in the source region systematic azimuthal bias may be introduced with stations in only a 180 degree sector around the source.

If we assume that all stations are at the same distance from the source with equal slowness values (i.e., $dT/d\Delta_k = P$), the determinant of S can be written as:

$$|S| = P^2 \left\{ \sum\cos^2(\phi_k) \right\} \left\{ \sum\sin^2(\phi_k) \right\} - \left\{ \sum\sin(\phi_k)\cdot\cos(\phi_k) \right\}^2$$

According to Cauchy's inequality the determinant is always greater than zero except when: $\sin(\phi_k) = c \cdot \cos(\phi_k)$, for all k, where c is a constant.

In order to study distributions with a maximum value of the determinant we write $x_k = \sin(\phi_k)$ and this gives the following expression for the determinant:

$$\left\{ \sum x_k^2 \right\} \left\{ \sum (1 - x_k^2) \right\} - \left\{ \sum x_k \sqrt{1 - x_k^2} \right\}^2$$

Rather than attempting to find the x_k values for a given n that maximize the determinant, we assume that the x_k are realizations of a stochastic variable ξ with the range of variation (-1,1). We also replace the summations with expectation operators, E, and get:

$$E(\xi^2) E(1 - \xi^2) - \left(E\left(\xi \sqrt{(1 - \xi^2)} \right) \right)^2$$

We are interested in finding the distribution of ξ that maximizes the expression above. For simplicity we assume that ξ is uniformly distributed over the interval α, β. In this case the determinant can then be written in a closed form:

$$\left\{ 1/9(\beta - \alpha) \right\}^2 \left\{ (\beta^3 - \alpha^3) \cdot (3(\beta - \alpha) - (\beta^3 - \alpha^3) - \left\{ (1 - \alpha^2)^{3/2} - (1 - \beta^2)^{3/2} \right\}^2 \right\}$$

For α and β we have:

$$-1 \leqslant \alpha \leqslant \beta \leqslant 1$$

Figure 1 shows the relative location error as a function of azimuthal coverage for a "uniform" distribution as defined above. The curve suggests that error decreases rapidly with increasing coverage at small values of the coverage and a coverage of 90 degrees gives an error about 20 percent larger than that with a coverage of 180 degrees.

2.1.3. Some Examples of Uniform Distributions

In order to study the effect of distance and azimuth coverage on location errors we calculate the location error for some hypothetical networks, which are distributed along circular arcs around the epicenter at various epicentral distances, i.e.,

$$\frac{dT}{d\Delta_k} = P(\Delta)$$
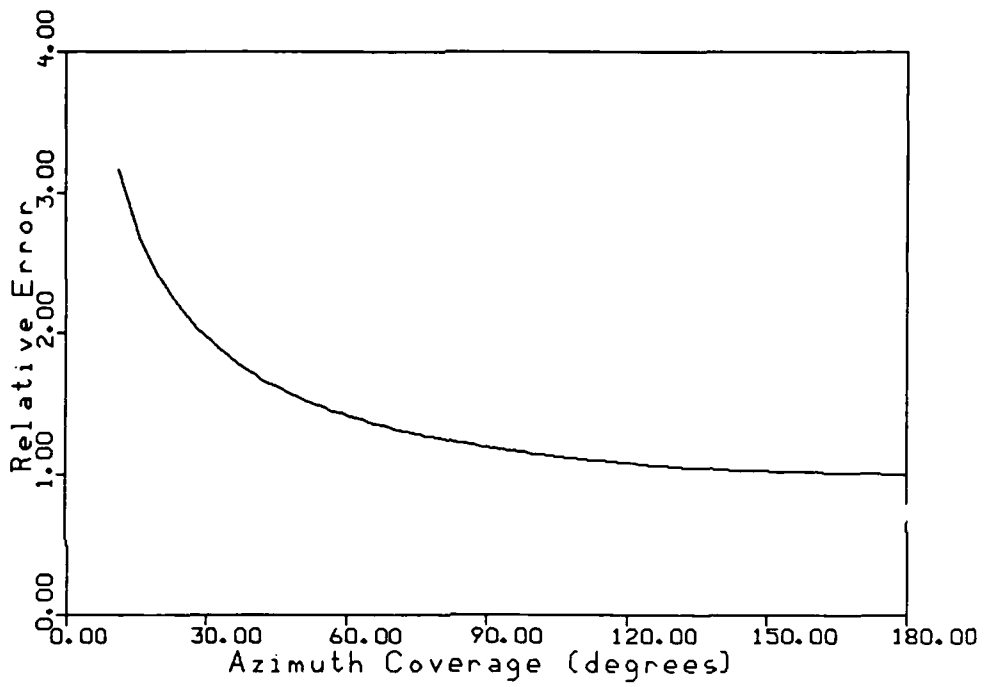
for all stations, k.

Figure 1. The curve shows the relative location error as a function of azimuth for a uniform station distribution represented by a stochastic variable as described in the text.

We assume that the event occurs at a depth of 1 km, and calculate errors for networks on arcs with a radius of 10, 20, 30, ..., 90 degrees. The length of the arc or the azimuth covered vary from 22.5 to 270 degrees. The number of stations in the networks are $n = 4,8,12,16,...,32$.

In this case the area of the error ellipse simplifies to the formula:

$$\pi \cdot \chi_2^{p} \cdot \sigma^2 |\, S\,| \,/nP(\Delta)$$

here the elements of the matrix S do not contain the slowness values. We note that the square root of the area of the confidence ellipse is inversely proportional to the slowness value and directly proportional to the *a priori* standard deviation.

In other words, the area of the location error is direct proportional to the number of stations, n.

Examples of some hypothetical networks with associated error ellipses are shown in *Figure 2*. The figure includes six networks distributed on circular arcs at 10, 20, 30, 50, 70, and 90 degrees with 4, 8, 12, 16, 20, and 24 stations with azimuthal coverage of 22.5, 45.0, 90.0, 135.0, 180.0, and 270.0 degrees. For example the network at 50 degrees consists of 16 stations covering an azimuthal sector of 135 degrees. The associated error ellipses are to the right in the figure. The two largest ellipses corresponds to the smallest networks with 4 and 8 stations. In can be seen that there is no dramatic difference in the area of the other four ellipses, which are associated with networks covering an azimuthal sector of 90 degrees or more.

The effect of azimuthal coverage on the location error can also be seen in *Figure 3*, which shows the error ellipses for 4 and 32 station networks both with the stations at 60 degrees epicentral distances and at varying azimuthal coverage from 22.5 to 270.0 degrees. In this case the effect of distance is kept fixed and the effect of number of stations is controlled by looking at extreme values. Again, it can be seen that there is no dramatic difference between the error ellipses for networks with a 90 degree or more coverage for a given number of stations. As expected, the number of stations affect the overall size of the error ellipses.

Figure 4 shows error ellipses for networks with a given azimuthal coverage (90 degrees) with the stations (in all 12) at different distances from 10 to 90 degrees in the left diagram, and with different numbers of stations (4 to 32) at a given distance (60 degrees) in the right diagram. The areas of these ellipses vary with the slowness as a function of epicentral distance and with the square root of the number of stations.

The location error as a function of azimuthal coverage, epicentral distance, and number of stations for concentric networks are outlined by *Figures 5-7*. In *Figure 5* the location error is shown for a 12 station network with azimuthal coverages from 22.5 degrees and distances 10 to 90 degrees. The location error drops about a factor of two as the azimuthal coverage increases from 22.5 to 120 or more degrees. The curves in
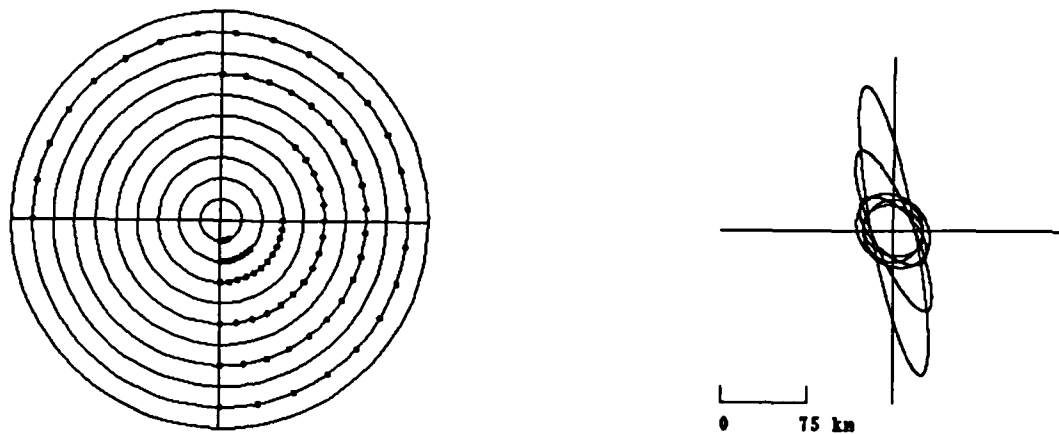
Figure 2. Examples of concentric station networks with 4, 8, 12, 16, 20, and 24 stations at epicentral distances 10, 20, 30, 50, 70, and 90 degrees, respectively, and with azimuthal sector coverages of 22.5, 45.0, 90, 135.0, 180, and 270.0 degrees (to the left). The figure also shows the associated error ellipses of the epicenter estimates (to the right). The two largest ellipses are associated with the networks of 4 and 8 stations.

Figure 3. The figure shows the error ellipses for concentral networks at 60 degrees epicentral distance and with 4 (to the left) and 32 (to the right) stations covering azimuthal sectors of 22.5, 45.0, 90.0, 135.0, 180.0, and 270.0 degrees. The two largest ellipses in each diagram corresponds to the networks with 22.5 and 45.0 azimuthal degree coverage.
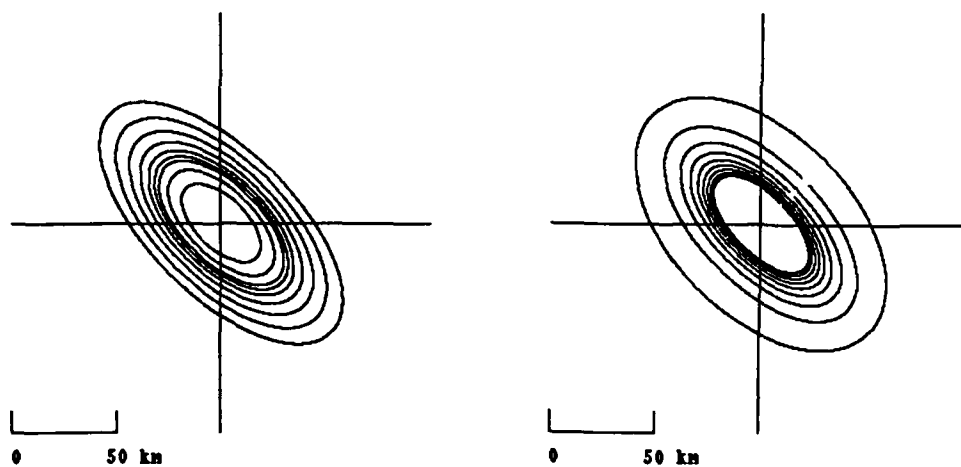
Figure 4. Error ellipses of concentral station networks with 90 degrees azimuthal coverage and with 12 stations at varying epicentral distances (10-90 degrees, to the left) and with varying number of stations (4-32) at 60 degree epicentral distance (to the right).
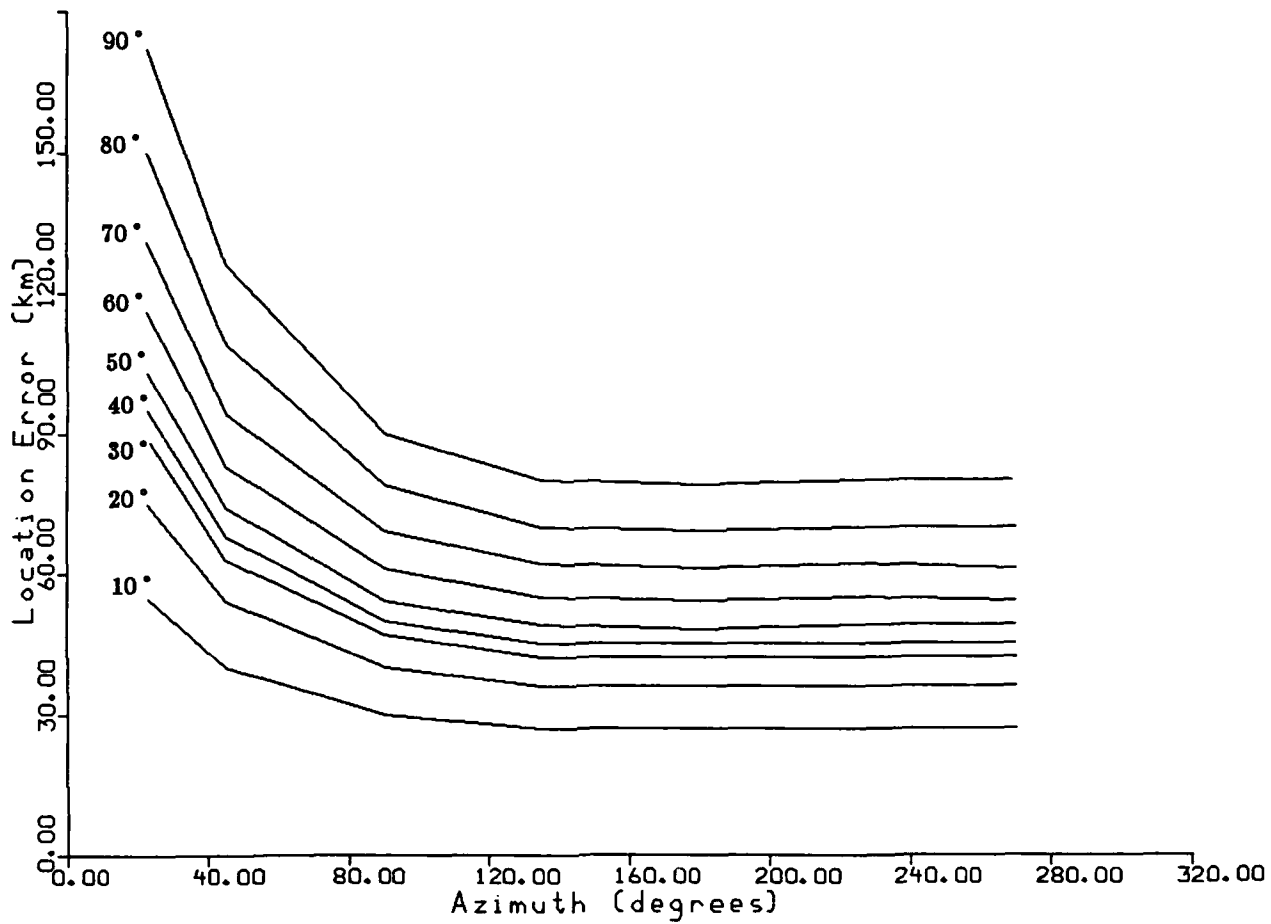
Figure 5. Location error as a function of azimuthal coverage for concentric networks with 12 stations at epicentral distances 10 to 90 degrees.
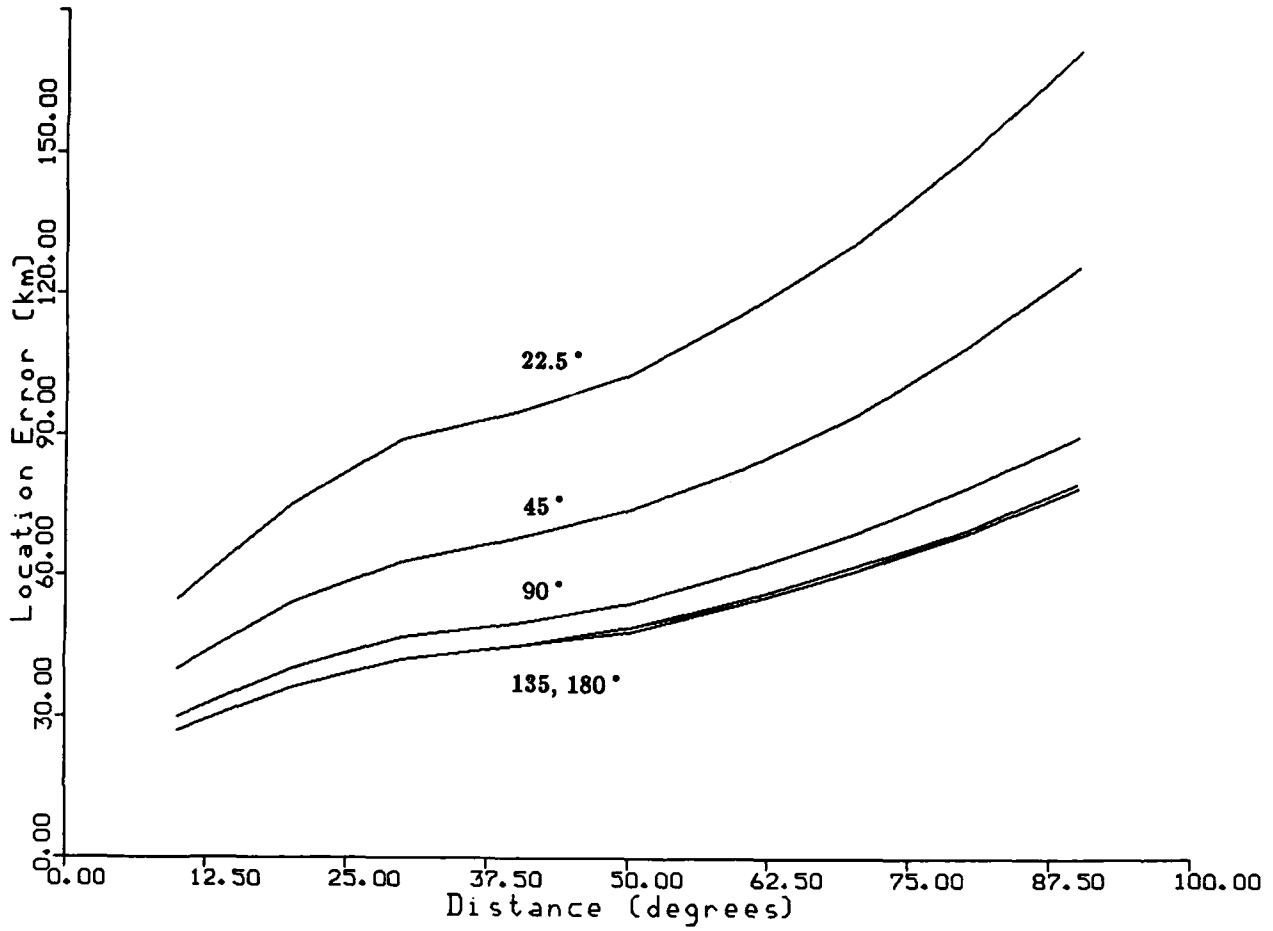
Figure 6. Location error as a function of epicentral distance for concentric networks with 12 stations and with azimuthal coverages of 22.5 to 180 degrees.
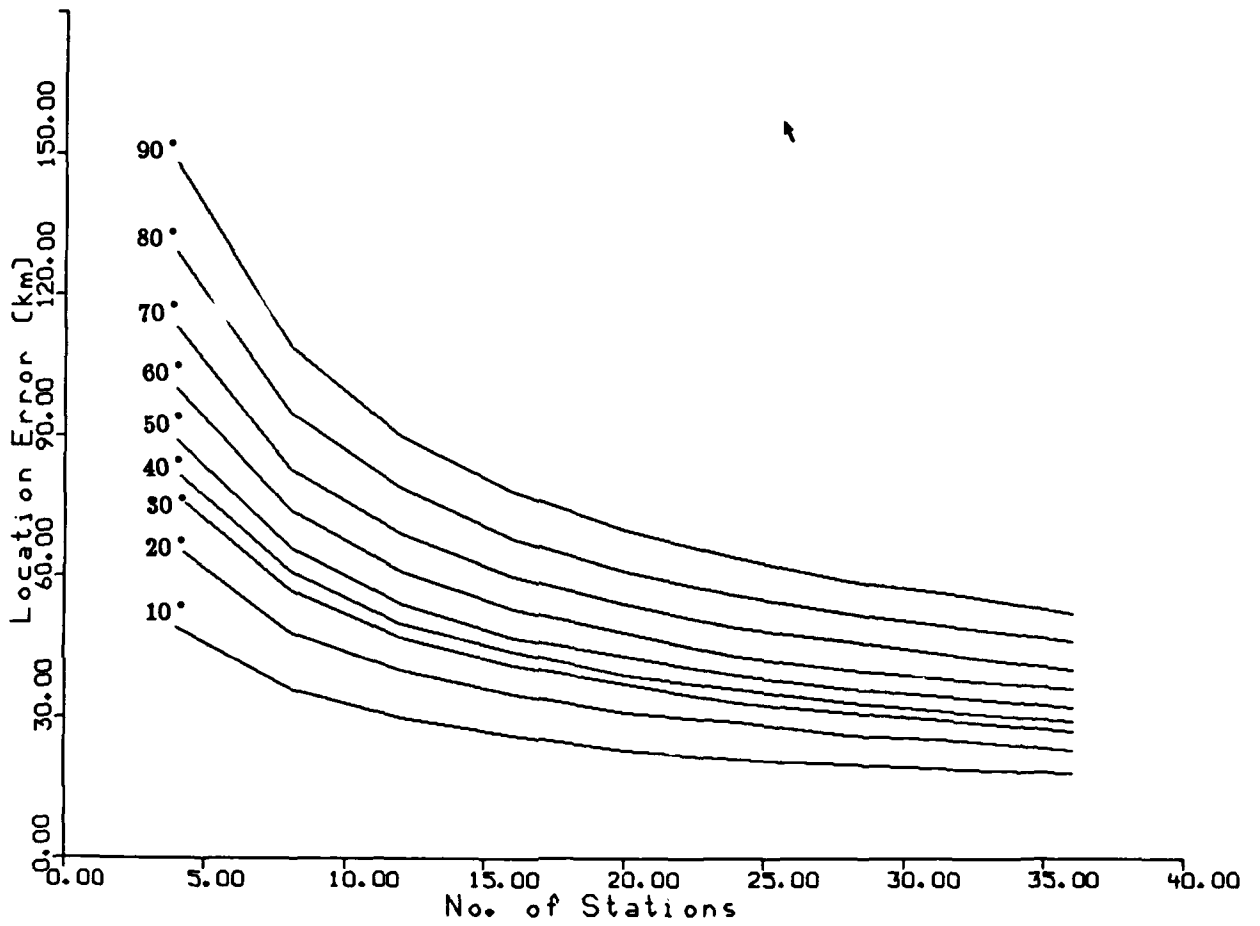
Figure 7. Location error as a function of number of stations for concentric networks with azimuthal coverages of 90 degrees and at epicentral distances of 10 to 90 degrees.

Figure 5 also shows an even more significant decrease (about a factor of three) in error as the epicentral distance of the concentric network decreases from 90 to 10 degrees.

The distance effect is also shown in *Figure 6*, whereas the error is shown for a network of 12 stations at azimuthal coverages from 22.5 to 180.0.

Finally, in *Figure 7* the error is shown as a function of number of stations for concentric networks with 90 degrees azimuthal coverage at distances from 10 to 90 degrees. A rather small reduction in location error is obtained for 15 stations or more.

2.1.4. Concluding Remarks

In this note we analyze epicenter errors for hypothetical network with regard to number of stations, azimuthal distribution, and epicentral distances with a standard statistical model. We use the *area* of the joint marginal confidence ellipse as a measure of the location error.

The errors due to azimuth distribution are periodic with a period of 180 degrees, i.e., an azimuthal coverage of 360 degrees around the epicenter does not provide smaller errors than a coverage of 180 degrees. For networks with a uniform distribution along an epicentral arc around the event epicenter a coverage of 90 degree gives errors which are not dramatically larger than those of networks with a complete 180 degree coverage. This conclusion is based on the particular assumptions about the model used; in practice, lateral velocity variations in the source region may introduce systematic azimuthal bias with stations covering a sector of 180 degrees or less.

The epicentral error is inversely proportional to the slowness for networks with stations at equal epicentral distance from the event.

The area of the location error is for such networks inversely proportional to the number of stations of the network.

Hans Israelsson

REFERENCE

Flinn, E.A., 1965. "Confidence Regions and Error Determinations for Seismic Event Location Reviews of Geophysics," 3: 157-185.

2.2.   A NOTE ON NETWORK DESIGN: STATION DISTRIBUTION FOR MINIMUM VARIANCE OF DEPTH ESTIMATES

2.2.1.   Introduction

Determination of focal depth is one important function of a seismological station network for test ban monitoring. Accurate depth estimates can be obtained on the basis of surface reflected phases, pP and sP. Unfortunately the frequency of reporting of surface reflections is usually quite low, and depth phases are also difficult to identify, in particular for shallow events. Even if the prospects for comprehensive use of surface reflections for depth determination appear rather limited, there are also studies that indicated that significantly improved observability may be obtained if waveform data from a network of stations can be analyzed simultaneously (Roy, 1984). Only systematic future attempts of utilizing such a network approach with waveform data for detection of surface reflections can confirm these promising tentative results. For the time being it appears that first arrival times of P-waves will be the most important information available for depth determinations, in particular for small magnitude events for which waveform data is nothing more than a small amplitude barely above the background noise. In this note we discuss the relative location of stations and seismic events for accurate depth estimation based on first arrival times.

2.2.2.   Model

We use a simplified approach to study the accuracy of depth estimates as a function of geographical distribution of stations (Lomnitz, 1977). It is assumed that the epicenter of the event is known, the focal depth will be estimated and that n stations have reported arrival times, t_{oi}, which all have an error with the same standard deviation σ. Forming the residual, $r_i = t_{oi} - t_{ci}$, between the observed and the calculated, (t_{ci}), arrival times, the following relations are obtained between the residuals, the adjustments in depth , dh, and in origin time $d\tau$:

$$r_i = d\tau + dh \left\{ \frac{dt}{dh} \right\}_i$$

This can be regarded as a straightforward linear regression relation and the variance of the estimated dh can be written as:

$$V(dh) = \frac{\sigma^2}{\sum \left(\left\{ \frac{dt}{dh} \right\}_i - \frac{\overline{dt}}{dh} \right)^2}$$

For standard travel time models the derivative $\frac{dt}{dh}$ is a function of epicentral distance Δ only for a given depth h. Examples of this derivative as a function of distance for the Jeffreys-Bullen travel time model for focal depths at 10, 30, 50, 100, 200 km are shown in *Figure 1*. The estimated curves were obtained by a bicubic two-dimensional spline approximation to Jeffreys-Bullen travel time tables. The curves for depths at 30 km and more are monotonically decreasing with distance with most of the decrease occurring at distances less than 20 degrees. Since the range of variation of $\frac{dt}{dh}$ is limited, the minimum variance of dh is obtained if all the stations are located at the boundaries of the distance interval over which they are distributed. In other words, if there are n stations (assume even number) that can be located anywhere within the distances interval Δ_{min} to Δ_{max}, the minimum variance is obtained if half of the stations are located at Δ_{min} and the other half at Δ_{max}, and the standard deviation of dh becomes:

$$\sigma(dh) = 2 \cdot \sigma \frac{(dt)}{\sqrt{n} \cdot (dt/dh(\Delta_{min}) - dt/dh(\Delta_{max}))}$$

2.2.3. Examples

The formula above for the variance of the depth estimate with stations symmetrically placed at the ends of the range of intervals covered has been used for a network of four stations, two placed at either end of the covered distance interval in *Figure 2*. Two of the stations are supposed to be at 80 degrees distance and the standard deviation is shown as a function of the distance of the two other stations (minimum distance) for events at 30 and 200 km depths. The standard deviation starts to increase significantly as the minimum distance becomes larger than 15 degrees or so. In fact, it is increased four times as it goes from 10 to 30 degrees. This illustrates the importance of one or more detecting stations at local or regional distance in a network based primarily on teleseismic detection.

If we assume that a network has a fairly equal station spacing on the globe we can ask for any given location what is the probability that stations within say 15 degrees do not detect an event and four or more stations at distances beyond 15 degrees do detect the event. This probability is denoted $P(\sigma_{large})$ below. In this case the standard deviation of the estimated depth would be fairly large, and a low probability is desirable. If we assume a network of N stations, the number of stations within Δ degrees is: $n(\Delta) = (1 - \cos(\Delta))/2 \cdot N$ for equal station spacing. The detection probability at station i as a function of magnitude is usually described by a normal distribution function and by the station threshold T_i and associated standard deviation σ_i: $p(m) = \Phi\left((m - T_i)/\sigma_i\right)$.

The probability mentioned above can be written as:

$$P(\sigma_{large}) = P(\xi \geqslant 4) \cdot P(\eta = 0)$$
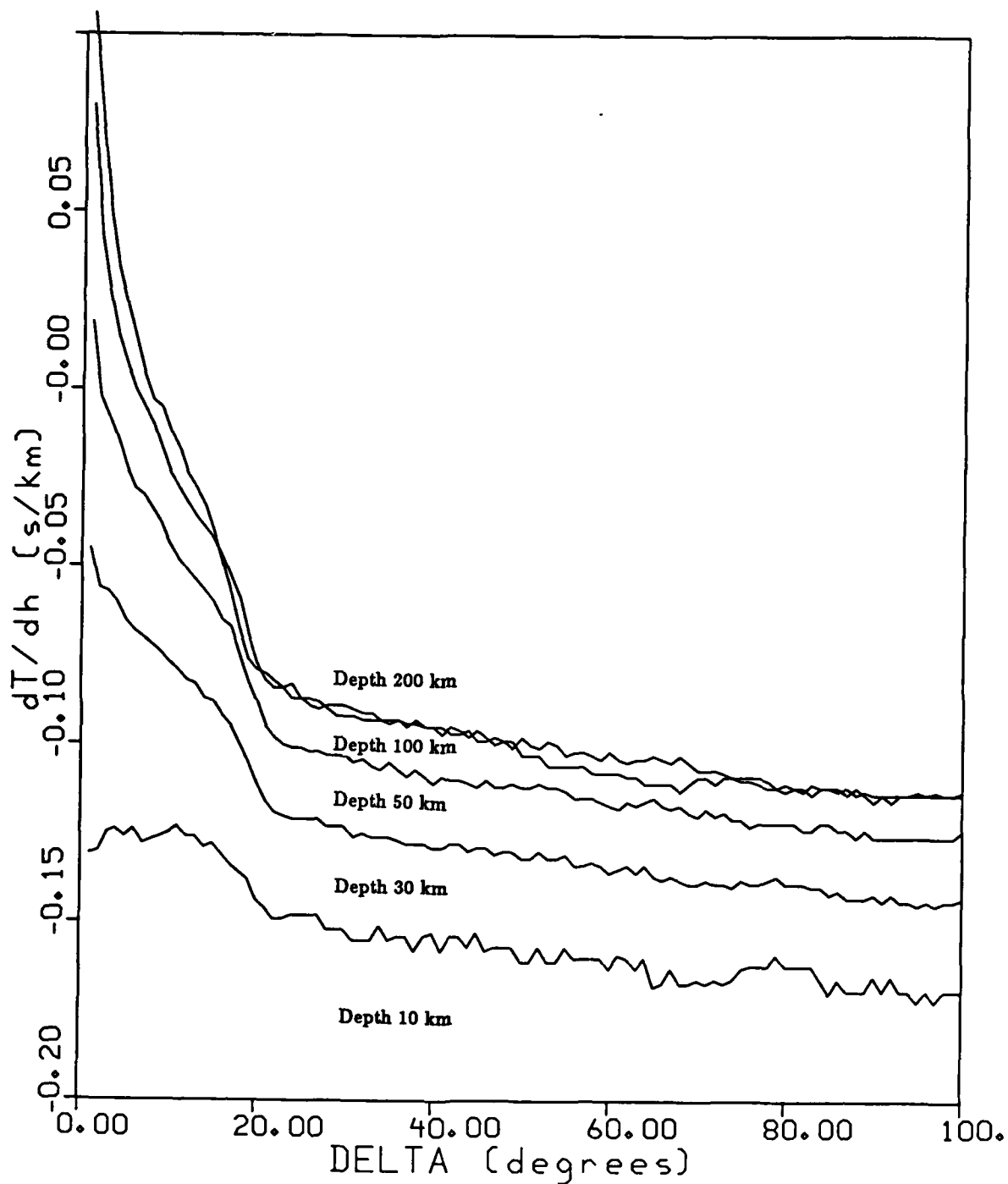
Figure 1. The travel time depth derivative, dt/dh, as a function of epicentral distance derived from the Jeffrey-Bullen P-travel time tables.
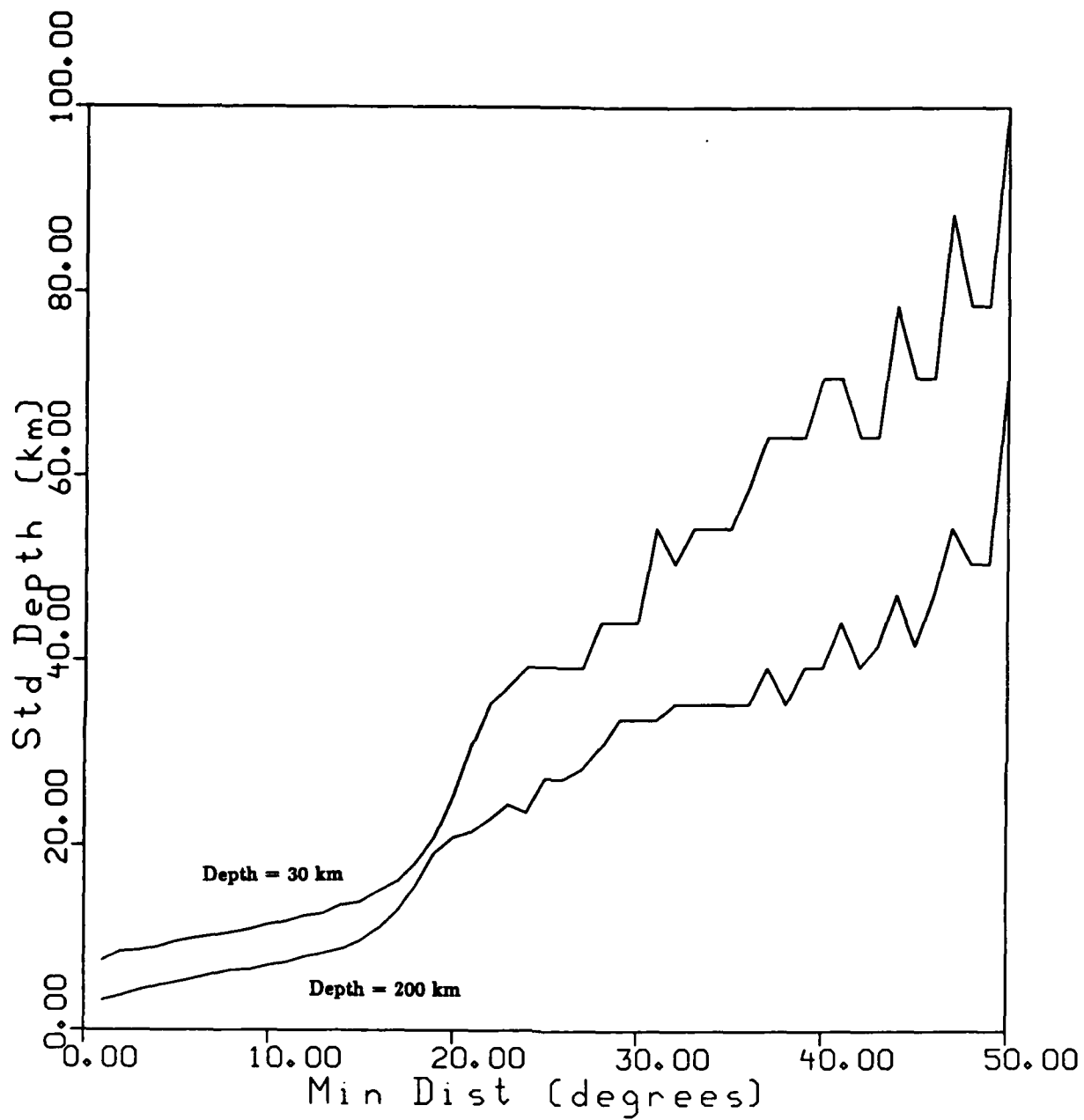
Figure 2. Standard deviation of estimated focal depth for events detected by four stations. Two stations are 80 degrees from the epicenter, and the other two are at various distances as indicated by the horizontal axis of the figure. Notice that the standard deviation increases rapidly as this minimum distance increases from 10 to 25 degrees.
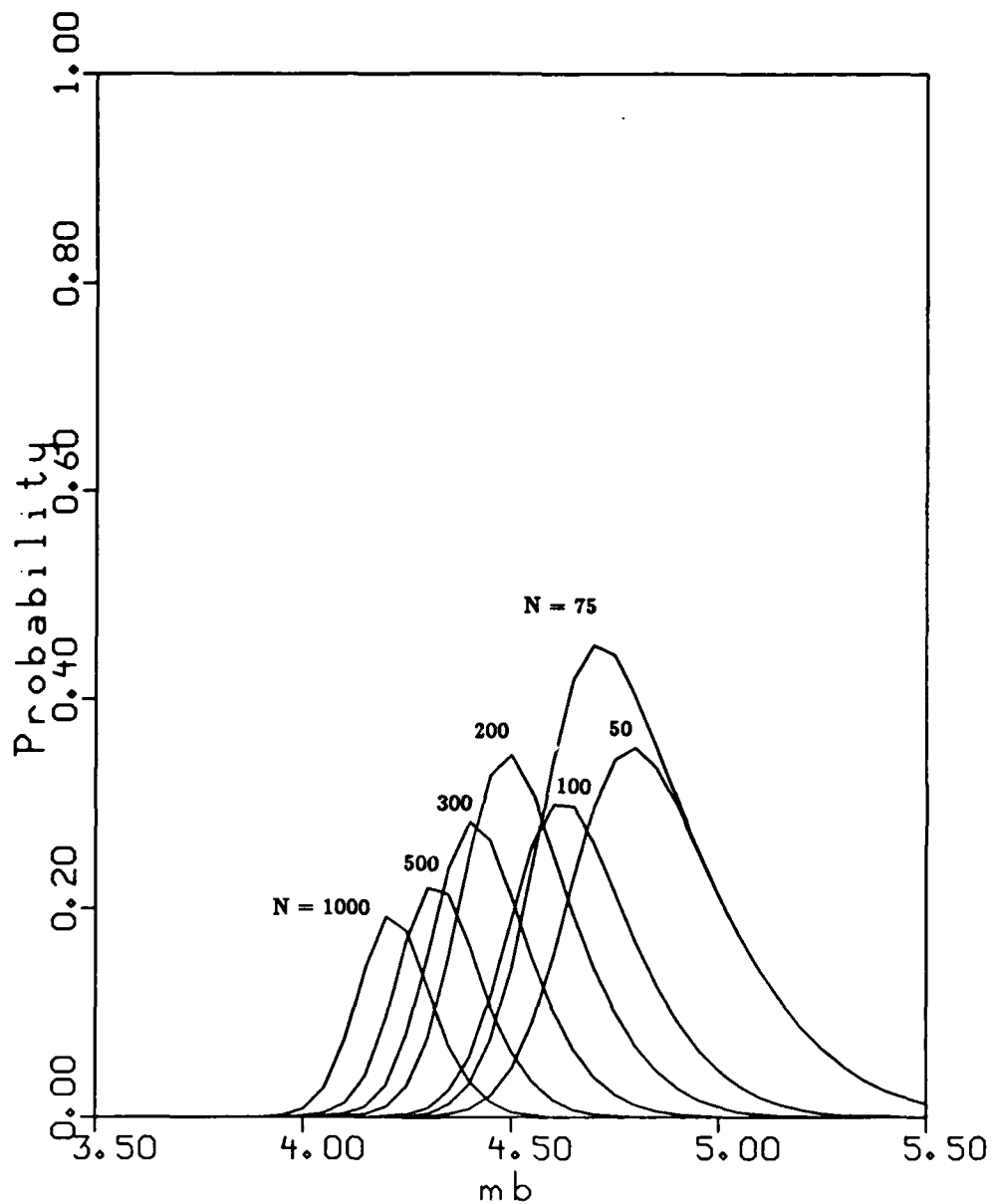
Figure 3. The diagram shows the probability that no station within 15 degrees from the epicenter detects an event and four or more stations between 15 and 80 degrees detect the event. The probability is shown as a function of magnitude for the events and for ideal networks with equal station spacing as described in the text.

where ξ and η are binomial stochastic variables for the number of detecting stations between 15-80 and less than 15 degrees, respectively. Assuming the thresholds T_i are 4.72 and 5.0 for station distance less than 15 and between 15-80 degrees, respectively, and $\sigma = 0.40$ we get the probability curves of *Figure 3* as a function of magnitude, m, for networks with $N = 50$ to 1000 stations. The recently suggested GSE concept network includes 50 fairly uniformly distributed stations. The curves suggest that a significant reduction of $P(\sigma_{large})$ is only obtained with increasingly large number of stations, several hundred or more for a complete coverage of the globe. If desirable coverage is limited to the continents these numbers would, however, be reduced accordingly.

2.2.4. Concluding Remarks

In this note we study the standard deviation of estimated focal depth on the basis of first-arrival times.

It is shown this standard deviation is entirely determined by the distance range covered but detecting stations. Coverage limited to the teleseismic range 30-80 degrees will give comparatively large standard deviations, whereas a significant improvement is obtained if observations at 15 degrees or closer can be utilized.

An example with idealized hypothetical networks suggests that global station networks need to consist of a large number of stations, several hundred, in order to achieve a comparatively low standard deviation of depth estimates for events throughout the world.

Hans Israelsson

REFERENCES

Lomnitz, C., 1977. "A Procedure for Eliminating the Indeterminacy in Focal Depth Estimation," *Bull. Seism. Soc. Am.*, 67: 533-536.

Roy, F., 1984. "Source Depth Estimation Using Multi-Station Waveform Data," *Bull. Seism. Soc. Am.*, 74: 1623-1643.

2.3. A NOTE ON NETWORK DESIGN: SHIELD AND PLATFORM NETWORKS

Seismological stations located on shields and platforms are often observed to have lower event detection thresholds than those for stations located in tectonically active regions. The simplicity of shield and platform structures also frequently results in comparatively simple recorded seismic signals which facilitates, for example, identification of depth phases and waveform analysis, which has become an important new element of the GSE-system. With these advantages to be accrued from shield and platform stations, we are exploring the capabilities of global networks composed of stations primarily located on shields and platforms. This note summarized the status of this investigation.

Shield and platform areas that have had seismological stations located in them are marked in *Figure 1*, which is based on a station list including about 4000 stations compiled at the Center for Seismic Studies, which in turn is primarily based on compilations by the USGS (USGS, 1985). There are 58 and 75 segments (five by 5 degrees in latitude and longitude according to regionalization by Jordan, 1984) with one or more stations for shield and platform regions, respectively. In all, this gives 133 segments with one or more stations. This number can be compared with the number (20) of shield and platform stations that participated in the GSETT.

Calculations of event detection capabilities and other seismological monitoring functions were made for several hypothetical networks including one consisting of 133 stations located at the segments where seismic stations have been in operation. For the sake of comparison, calculations were made for networks with 25 - 175 stations more uniformly distributed over the shield and platform areas, and for a hypothetical version of the GSETT network (total of 69 stations) and the GSE concept network (GSE/US/44, 1987). The latter consists of 50 stations, eight of which have arrays. The same station parameters were used for all networks (the only exceptions were the eight array stations of the concept network, which were given a short-period noise amplitude of 2 nm instead of 10 nm). Notice that the noise amplitudes assumed for the GSE concept network here are a factor of two larger than those used in earlier calculations (GSE/US/44, 1987). The calculations assumed only teleseismic observations, i.e., use of regional phases, which are particularly important for depth estimation was not included.

Examples of calculated event detection thresholds are shown in *Figures 2* and *3*. The contours of the 90% m_b- threshold for the GSE concept network are compared with a 99-station network on shields and platforms in *Figure 2*. The threshold for the concept network varies much less (4.4-4.6) than that for the 99-station network (4.2-4.8). However, the threshold of the 99-station network is below 4.4 for most of the continental areas. *Figure 3* summarizes the m_b thresholds for the networks. The figure suggests that no significant lowering of the world average threshold is achieved by increasing the number of stations beyond 75 or so for shield/platform networks. The concept network has a fairly small range of variation, as would be expected from *Figure 2*. The GSETT network has a larger range of variation, primarily because of the concentration of stations in Europe. The GSETT network also has lower maximum threshold than that of 75 shield/platform stations, owing to some oceanic stations.
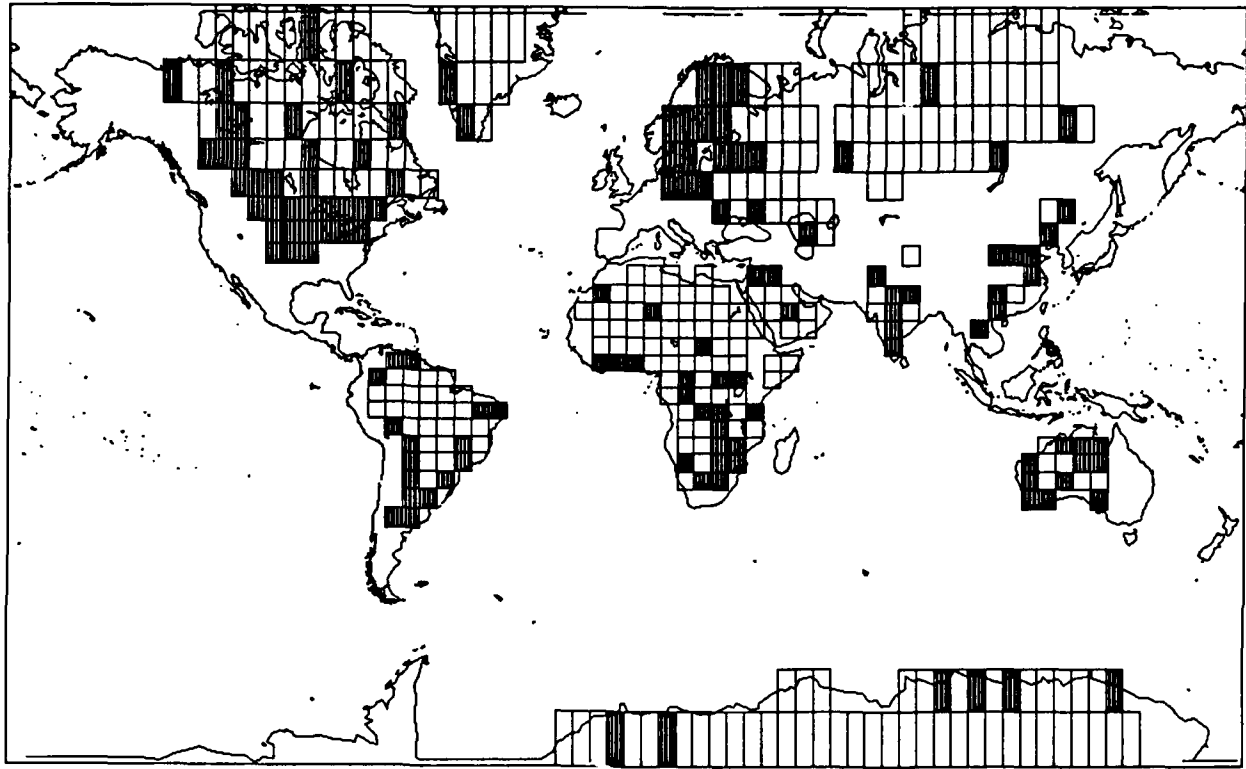
Figure 1. The map shows the shield and platform segments on which one or more seismological stations are or have been operating (indicated as filled rectangles).
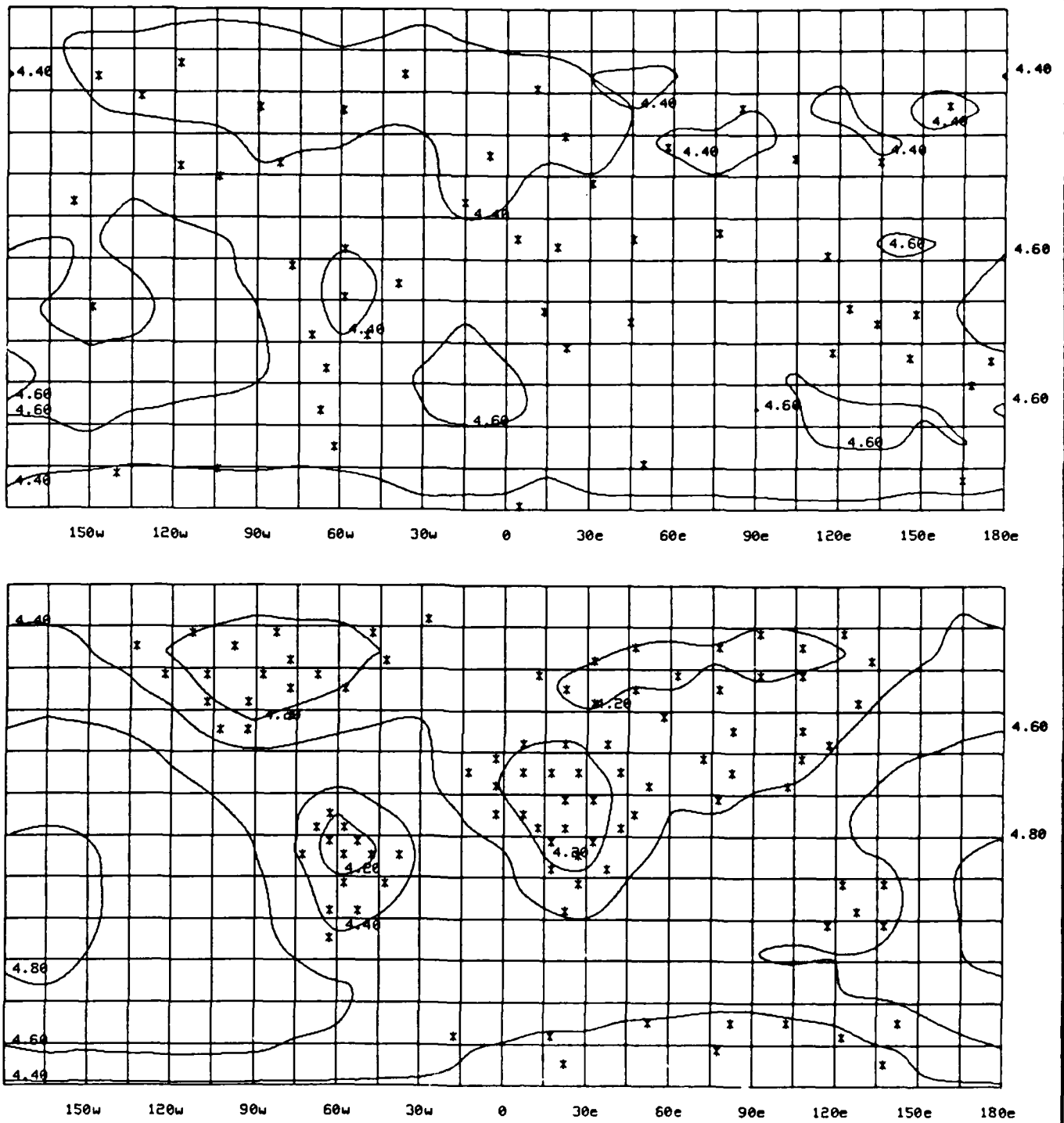
Figure 2. Contours of the 90% m_b-detection threshold for the GSE concept network (top) and 99-station shield/platform network (bottom). *P*-signal detections at four or more stations are used as event detection criterion.
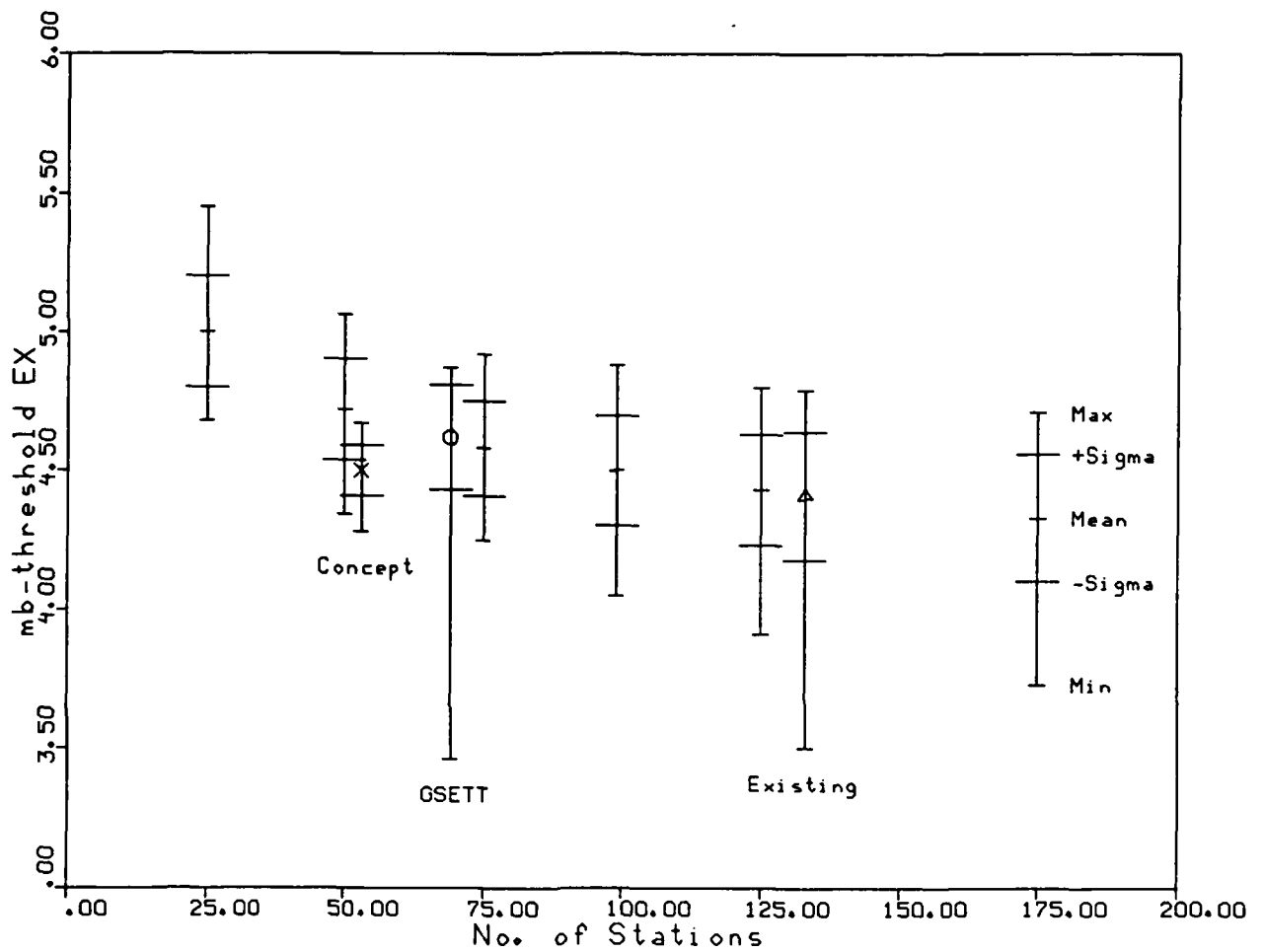
Figure 3. Detection threshold, m_b, as a function of number of stations for shield/platform networks. The diagram shows mean, range of variation (minimum and maximum), standard deviations (plus and minus mean) for each network as indicated for the 175-station network to the right in the diagram. Results are also included for the GSE concept, the GSETT networks and a hypothetical 133-station network of existing stations as marked in the figure. The GSE concept network which includes 50 stations have been displayed slightly to the right in the diagram for sake of clarity.

2-22

In conclusion, the shield and platform networks seem to have nonuniform capabilities on a global scale for basic seismological functions. This is not as pronounced for event detection and M_s-determination and is comparable to other existing networks, but is very clear for location and depth. There seem to be reasonable capabilities on the continents, provided sufficient number of uniformly distributed stations would be available. It appears that a network with reasonably uniform coverage cannot be based entirely on stations in shield and platform areas. Such a network would, however, be sufficient for uniform coverage of the territorial areas on the major continents. The GSE concept network, including 50 stations, provides fairly uniform global coverage for event detection, location, and M_s-determination. The depth estimation capability is, however, more limited in particular for shallow focus explosions. Some of the limitations of depth estimation capability may be improved by use of waveform data and use of local and regional phases.

Hans Israelsson

REFERENCES

GSE/US/44, 1987. "Technical Concepts for a Global System for Seismic Data Exchange," *United States Delegation to the Conference on Disarmament, Geneva, Switzerland.*

Jordan, T. H., 1981. "Global Tectonic Regionalization for Seismological Data Analysis," *Bull. Seism. Soc. Am.*, 71: 1131-1141

USGS, 1985. "Seismograph Station Codes and Coordinates National Earthquake Information Center," *USGS Open-File Report*, 85-714.

3. RESEARCH TO IMPROVE ANALYSIS OF REGIONAL SEISMIC DATA

3.1. CHARACTERISTICS OF REGIONAL SEISMIC PHASES RECORDED BY THE NORESS ARRAY

3.1.1. Introduction

In previous technical reports, we have presented papers outlining the development of a number of processing methods for the extraction of signal parameters from NORESS data. These analyses include frequency-domain spectral parameters, time-domain autoregressive (AR) parameters, and particle-motion information. These methods are now being used at the Center to test their applicability to the problem of regional wave propagation and seismic discrimination, in particular the discrimination of small chemical explosions from natural microearthquakes ($M_L < 3.5$). The dataset we are testing includes approximately 100 events in Scandinavia and the western Soviet Union. To date, approximately 50 events have been analyzed in detail. In this paper, we present some preliminary results of our study. Our goal is to review the characteristics of the regional seismic phases P_n, S_n, and L_g. We will focus on the frequency content, Q estimates, and the three-component characteristics of these phases.

3.1.2. Signal Processing

Power spectral estimates of the NORESS data are performed interactively with a Sun Microsystems workstation. The central (NRA0) channel is displayed in a number of frequency bands and the times of P_n, S_n, and L_g are chosen. Then these time picks are used to retrieve the data from the 25 vertical channels. To obtain an initial estimate of the peak frequency and shape of the spectra, the multichannel data are modelled as a damped harmonic oscillator (DHO) by a method described by Dysart (1986). The peak frequency and damping factor of the equivalent DHO are useful in describing the spectral content of a signal in terms of the least number of physically significant parameters. Power spectral estimates are also determined for the whole array by averaging the spectra from each vertical channel. This averaging procedure reduces the variance in spectral amplitudes and results in a spectral estimate similar to a conventional periodogram. The peak frequency is obtained from the instrument-corrected velocity spectrum. Spectral amplitudes above a preset signal-to-noise ratio are then fit to an idealized source function to obtain estimates of the attenuation factor Q, and the corner frequency.

Particle-motion information is extracted using all the three-component sensors in the array by the method described by Jurkevics (1986a, 1986b). In this approach, the covariance matrices from all three-component sensors are computed in the time-domain and averaged together, and the usual eigenproblem is solved to obtain the polarization ellipse as a function of time. Particle motions are characterized by various attributes of the polarization ellipse. In this analysis a time pick was made interactively on each of the regional phases of a seismogram and several particle-motion attributes extracted in a

short-time segment in fixed frequency bands centered at 4, 6 and 10 Hz. The time segments vary in length in order to isolate the most stable particle motions characteristic of each phase.

3.1.3. Pn

For all of the events examined, the peak frequency of the P_n wave was greater than or equal to the peak frequency of either S_n or L_g. Magnitudes of the events studied range from 1.8 to 4.8 (M_L) with P_n peak frequencies ranging from 2.0 to 10.0 Hz. The variation of P_n peak frequency versus magnitude does not appear to follow a systematic pattern, but P_n peak frequencies and corner frequencies both show a dependence on distance. Peak and corner frequencies for close events are generally higher than those found for the more distant events. *Figure 1* shows the peak frequency versus distance for all three regional phases. This trend in peak frequency versus distance is consistent enough to note even though events of the same magnitude and distance can have significantly different P_n peak frequencies. For example, two explosions of magnitude 2.6 at a distance of 8 degrees can have peak P_n frequencies of 2.0 or 10.0 Hz. Whether this is a source effect or a path effect is yet to be determined. Regional dependencies certainly exist. Earthquakes on the west coast of Norway have high P_n frequencies (~10 Hz) whereas similar sized events at the same distance in Sweden are of lower frequency (~4 Hz).

Q estimates for P_n are generally high, with no obviously azimuthal dependence. Refinement of the estimation procedure and the addition of more events should resolve any existing trends as yet unseen.

The P_n waveforms for some explosions are highly monochromatic, arriving as a wave packet. This may be caused by delayed firing of charges, resulting in constructive interference at specific frequencies. Cepstral analysis of these waveforms suggest the presence of multiple sources separated by approximately 0.3 seconds. The presence of multiple cepstral peaks shows promise as a means of identifying mine blasts, however, the interference pattern of peaks and troughs seen in the spectra of these events can severely bias estimates of the corner frequency and Q.

P_n particle motion tends to be very rectilinear for a few seconds immediately following the initial onset. P_n polarization is stronger at higher frequencies (around 10 Hz) whenever there is a good signal-to-noise ratio in this band. The polarization structure of the coda waves following the initial P_n arrival deteriorates in time so that the late P-coda signals just prior to the S_n arrival have particle motions essentially like that of ambient noise. This P-coda polarization degrades more rapidly at higher frequencies, and the duration of the initial P_n strong rectilinear motion decreases with increasing source distance. If the events are within about 500 km then a series of strongly-polarized arrivals may be present in the early P-wave coda within 20 seconds of P_n, corresponding to a series of P_g waves trapped in the crust.
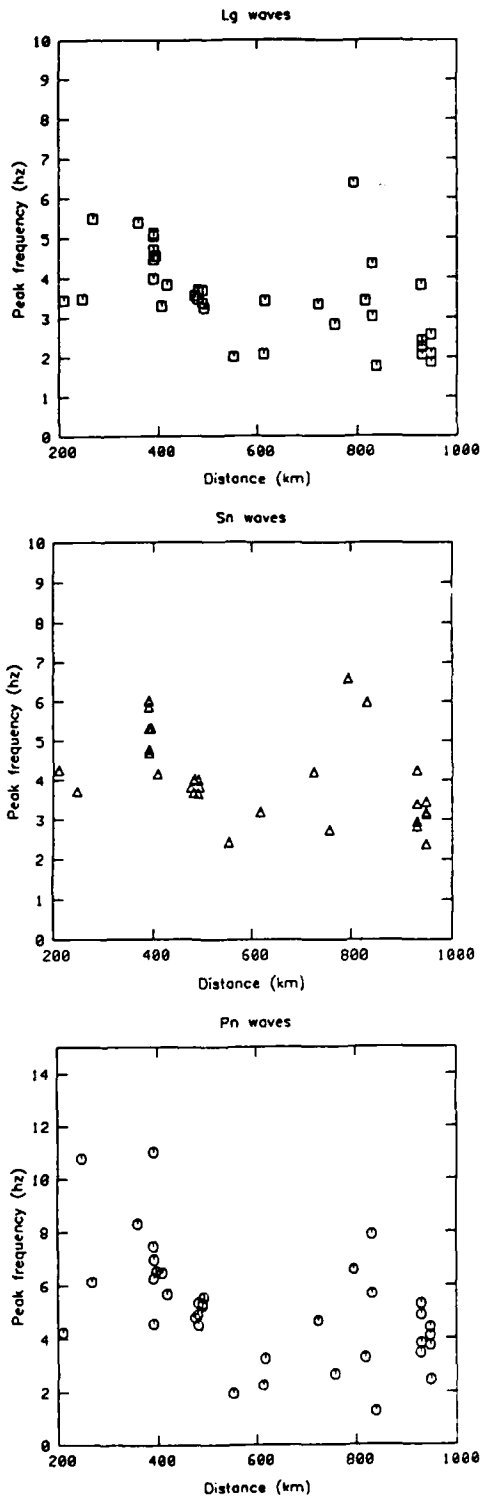
Figure 1. Peak frequency versus epicentral distance for P_n, S_n, and L_g phases.

Polarization attributes of the P_n motions were extracted at the time the signal amplitude and rectilinearity were highest. For a displacement signal-to-noise ratio (S/N) greater than about 2, P_n can be confidently distinguished from noise and L_g waves on the basis of rectilinearity. However, S_n also tends to be somewhat rectilinear and may be confused with P_n on this basis, depending on the signal-to-noise ratio. The best way to separate P_n from noise, S_n and L_g appears to be simply the vertical-to-horizontal ratio (V/H) at the highest frequencies for which the signal-to-noise ratio of P_n is greater than about 1.5. *Figure 2* shows a plot of log(V/H) *versus* log(S/N) for about 40 regional events recorded at NORESS. The signal-to-noise values in *Figure 2* are in amplitude units and the vertical-to-horizontal ratios are in units of power. Here the parameter V/H is computed as $2V^2 / (E^2 + N^2)$, where V, E and N are the vertical, east and north amplitudes, respectively. Using the orientation of P_n rectilinear motion, source back azimuths can be estimated to better than $\pm 20°$ in about 90% of the cases when the S/N amplitude is greater than about 1.5.

3.1.4. Sn

Peak frequencies of S_n waves were in all cases less than those of P_n and greater than those of L_g. These ranged from 1.5 Hz to 9 Hz. As with the P_n waves, systematic variation with magnitude did not show up in our dataset although there is a weak dependence on distance as seen in *Figure 1*. The characteristics of the S_n waves generally followed those of their associated P_n. For example, when the P_n peak frequency was high, the S_n peak frequency was similarly high. Thus, regional dependencies hold for both phases. It is interesting to note that explosions with highly monochromatic P_n waves had S_n waves with very similar spectra. Considering that P_n and S_n follow nearly identical wave paths in the Earth, this suggests that source effects may play a prominent role in the character of regional phases. Q estimates for S_n are consistently high as with P_n but are not discernibly different from those for P_n or L_g due to the high variance associated with the estimates.

Like P_n, the S_n particle motions are strongly polarized over a short-time interval of only a few seconds. S_n polarization is generally not as strong or well-defined as P_n polarization. However, the analysis carried out so far indicates that S_n can be distinguished from the other regional phases including L_g with a high degree of confidence using particle-motion information. The S_n phase is more emergent than P_n, and its signal-to-noise level is often lower than that for P_n, since it is the late P coda waves which control the effective background noise for S_n. S_n polarization is generally strongest at or just prior to the peak three-component envelope of this phase. Generally, S_n particle motions are somewhat better defined at the higher frequencies than at the lower frequencies (i.e., better at 10 Hz versus 4 Hz).

The dominant particle-motion characteristic observed for S_n is the large horizontal motion relative to vertical. *Figure 2* shows the vertical-to-horizontal ratios measured for S_n to be well below 1.0 and a function of the signal-to-noise level. The scatter is quite large, and the vertical-to-horizontal ratio in itself does not reliably distinguish S_n from L_g.
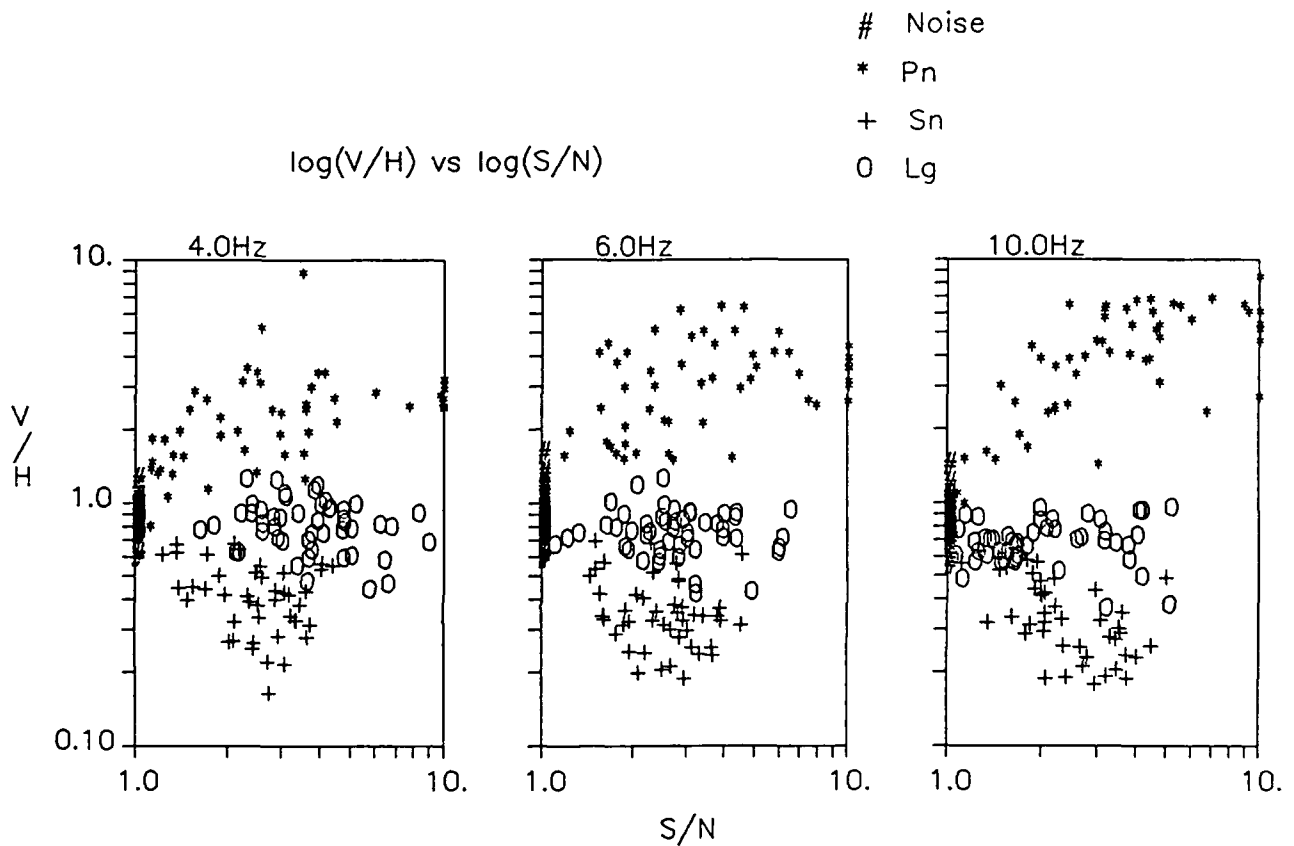
Figure 2. Vertical-to-horizontal ratios of regional phases computed from three-component seismograms. Results are plotted in three separate frequency bands as a function of the signal-to-noise ratio in each band. P_n waves tend to have V/H ratios greater than 1.0, S_n waves have V/H ratios less than 1.0, and L_g waves are similar to the ambient noise with a V/H near 1.0.

The radial motions for S_n are generally about equal to or slightly less than the horizontals. This means that S_n in not very useful for estimating source azimuth. The near-equal horizontals and smaller verticals gives S_n a polarization structure which is planar by nature, with this plane of motion oriented close to horizontal. This implies that the steeply-incident S_n waves contain both S_H and S_V components, with the S_H or transverse component somewhat larger in many cases.

3.1.5. Lg

Peak frequencies of L_g waves ranged from a low of 1.5 Hz to a high of about 6 Hz, however, the cases with high frequencies were very limited. Since L_g consists predominantly of S-waves traveling and reflected within the crust, they are highly path sensitive as compared with P_n and S_n. A separation in peak frequency between explosions and microearthquakes of the same magnitude did not show up. As for the preceding phases, Q estimates are high, and peak frequencies show a dependence on distance (*Figure 1*).

The L_g wavetrain is generally longer and more complex than the other phases, with a gradual increase in the envelope before the peak amplitude is reached. L_g particle-motions are quite variable with time, and the most consistent motions are found around the time of the envelope maximum. Since this phase is longer duration, a longer window was used to extract L_g particle-motion information than was used for P_n or S_n. *Figure 2* shows that the vertical and horizontal amplitudes of L_g tend to be about equal, which is also true of ambient noise. However, a characteristic feature of L_g motions is the dominance of vertical and transverse components relative to the radial. This means that, like S_n, the L_g polarization structure is relatively planar. Unlike S_n, the orientation of this plane of motion is dominantly vertical and transverse rather than horizontal. The analysis carried out so far indicates L_g can be separated from S_n on the basis of the orientation of this plane of polarization, or, equivalently, on the basis of the radial-to-vertical amplitude ratios. Such observed L_g polarization structure is consistent with the theory that the L_g wavetrain in the short-period band is comprised of trapped S waves propagating relatively horizontally in the crust with both S_V and S_H present.

The dominance of transverse motion for L_g implies that the source azimuth can be estimated using the orientation of minimum horizontal motion. The minimum axis of the polarization ellipse computed from only the horizontal components has been previously used to estimate the source back azimuth (to within $\pm 180°$), (Smart and Sproules, 1981). Preliminary analysis of regional events at NORESS indicates that the source azimuth can be determined this way to within about 20° in more than 75% of the cases when the S/N of L_g is greater than 1.5. Thus, the source azimuth estimates from L_g are not as accurate as those obtained from the P_n motions.

A. Jurkevics, P. Dysart and J. J. Pulli

REFERENCES

Dysart, P. S., 1986. "Autoregressive Analysis of Regional Seismograms from Earthquakes and Explosions," *SAIC/Center for Seismic Studies Technical Report for the Period 1 July - 30 September 1986*, C86-07, dated November 1986.

Jurkevics, A., 1986. "Polarization Analysis Using an Array of Three-Component Sensors: Part I — Theory," *SAIC/Center for Seismic Studies Technical Report for the Period 1 July - 30 September 1986*, C86-07, dated November 1986.

Jurkevics, A., 1986. "Polarization Analysis Using an Array of Three-Component Sensors: Part II — Application to NORESS," *SAIC/Center for Seismic Studies Technical Report for the Period 1 July - 30 September 1986*, C86-07, dated November 1986.

Smart, E. and H. Sproules, 1981. "Regional Phase Processors," *Teledyne Geotech Report*, VSC-TR-81-19.

4. INTERNATIONAL DATA EXCHANGE

4.1. GSE WAVEFORM EXCHANGE EXPERIMENTS

4.1.1. Introduction

Recent activities of the GSE in Geneva have accelerated the development of capabilities to exchange seismic waveforms. A data format tentatively approved by the GSE in August 1986 was reviewed and revised during the latter part of 1986 and the final version was distributed to GSE members in late December 1986.

This report documents waveform exchange experiments and related activities conducted by the Center during the first quarter of 1987 in order to gain experience with the proposed procedures and formats, and provides observations of Center personnel on the various exchange procedures.

4.1.2. Waveform Data Exchange Methods

The Center has conducted experiments employing all of the digital waveform exchange methods proposed by the GSE. These have included transfers by magnetic tape, electronic mail and direct computer-to-computer file transfer. The waveform data transfers are summarized in Table I. Each exchange method has its advantages and disadvantages, and these are discussed briefly here. It should be noted that the way in which a transfer is carried out can have profound implications for cost, reliability, data quality, and handling of the received data files.

The WMO/GTS has been used for years to transfer amounts of data that are small in comparison to useful seismic waveforms, and it was used exclusively for the exchange of parameter data during the GSETT experiment in 1984. It is straightforward to broadcast copies of data to many nations over the WMO/GTS network. There are doubts that the WMO/GTS will be able to handle the volume of data that would be expected from a large-scale exchange of waveforms. Furthermore, since the WMO system does not have error correction capability, and waveform data is useless unless almost error free, data integrity could be a serious problem.

Use of electronic mail (E-mail) networks has been limited by computer compatability and the coverage of the individual networks. E-mail can be transferred over standard telephone lines or packet-switched networks, and it works as long as there is a path and address available to the sender. Use of E-mail systems can reduce costs by permitting scheduling of transfers to take advantage of periods of low transmission rates and by spooling transfers. Electronic mail systems can also incorporate data compression and quality assurance algorithms.

Table I

INTERNATIONAL WAVEFORM EXCHANGE EXPERIMENTS
WITH UNITED STATES PARTICIPATION
(Jan - Mar 1987)

COUNTRY	REC'D/TRANS	TRANSMISSION		QUANTITY	EVENT	DATA		FORMAT	COMMENTS
		METHOD	RATE			SP	LP		
Austria	R	1600 bpi tape	--	10 Kbytes	84338	Z	--	GSE	
Canada	R	1600 bpi tape	--	100 Kbytes	84335	Z	Z,N,E	GSE	
	R	X.25	Unknown	100Kbytes	84335	Z	Z,N,E	GSE	We retrieved from their machine
Czechoslovakia/ Poland	R	800 bpi tape	--	2.5 Kbytes	84338	broadbd, Z,N,E	Z,N,E	non-GSE	
Denmark	R	X.25	Unknown	27 Kbytes	84338	Z	--	GSE	They delivered to our machine
Fed. Rep. of Germany									
Hannover	R	X.25(email)	Unknown	98 Kbytes	84338	Array	--	GSE	They delivered via Email
Italy	R	1600 bpi tape	--	46 Kbytes	84342	Z	--	GSE	
Japan	T	X.25(Kermit)	25 Bytes/sec	50 Kbytes	84301	Z	Z,N,E	GSE	We delivered to their machine
	T	X.25	500 Bytes/sec	50 Kbytes	84301	Z	Z,N,E	GSE	We delivered to their machine
	R	1600 bpi tape	--	600 Kbytes	84338	Z,N,E	Z,N,E	GSE	
					84339	Z,N,E	Z,N,E	GSE	
					84345	Z,N,E	Z,N,E	GSE	
					Unk	Z,N,E	Z,N,E	GSE	We retrieved from their machine
Norway	R	X.25	Unknown	80 Kbytes	84339	Z	--	GSE	They delivered to our machine
Sweden	R	1600 bpi tape	--	35 Kbytes	84338	Z	--	GSE	
		X.25	--	500 Kbytes	84339	Z	--	GSE	
	R	X.25	Unknown	230 Kbytes	84338	Z	--	GSE	They delivered to our machine
					84339	Z	--	GSE	
United Kingdom	R	X.25	Unknown	20 Kbytes	84338	Z	--	GSE	They delivered to our machine
					84339	Z	--	GSE	
					84345	Z	--	GSE	

Direct computer-to-computer transfers (excluding E-mail) are usually initiated by an individual while logged onto a remote computer. This method of transfer can be wasteful for a number of reasons. First, every user must have login capability and, depending on transfer direction, write permission on the remote machine. Second, transfers of this type, once initiated, tie up terminals, ports and people. Computer-to-computer connections designed for human interaction frequently are set up to pass each character as it is typed. This can cause packet-switched network charges to be orders of magnitude higher than they might otherwise be if the connection was optimized for transfer without interaction. Third, unless files are kept small or another layer of protocols are used (e.g., KERMIT), retransmission costs can be significant. Thus, this method of transfer can increase the data auditing task associated with exchanges. Since this method allows a user to initiate a transfer to his own machine while logged in on a remote machine, it introduces an additional class of transfer which contributes to an existing problem concerning all transfers. That is, having the final destination and name of the data be independent of the transmission method. A solution to this problem is outlined in a subsequent section. Finally, magnetic tape, although a delayed method for transferring data, is widely used and highly reliable and does not require special communications facilities or on-line storage which may be a problem for some centers. The cost of tape transfer is competitive with machine-to-machine transfers.

4.1.3. Data Requests and Exchanges

Although it is expected that the exchange of waveforms will be initiated by a formal data request, and the GSE has specified a format for data requests as well as for the data itself, most of the trial exchanges were not initiated with a formal request. The Center received only one request in GSE format and that came from Japan. The request was incomplete and a clarification was requested. The clarification was also incomplete since the time given was arrival time rather than start time and no window lengths, or phase names provided. But some assumptions were made and the requested data were E-mailed to Japan's account on seismo within hours. Similarly, data transfers to the Center resulted from a non-standard blanket request for waveform data from three widely recorded earthquakes. The request was forwarded along with tapes containing waveform data in GSE format, which were distributed to all GSE members in January 1987 for format evaluation. It was this blanket request which produced the exchanges summarized here.

Table I summarizes waveform exchanges which occurred during the first quarter of 1987. Information on the quantity of data transmitted, the transmission rate where it could be determined, method of transmission and event(s) for which data were transmitted are included in the summary. The events are designated by the year and day of year. Table II gives detailed information on the events selected for waveform data exchange. The Center received five GSE format exchange tapes. A non-standard format tape was also received from Czechoslovakia. The GSE tapes and their contents are tabulated in Table III. The entries are images of the GSE standard waveform identification header which begins with the character string WIDn and gives the event date, start time, number of samples, station name, channel identifiers, sample rate, instrument type and data format type. Waveform files that have been delivered, retrieved or E-mailed to seismo are tabulated in Table IV.

Table II

EVENTS USED FOR WAVEFORM EXCHANGE

Year/Day	Date	Origin Time	Latitude	Longitude	Region	M_b
84301	Oct 27, 1984	17:16:04	21.6S	139.4W	Tuomoto Arch	4.1
84338	Dec 03, 1984	04:08:35	44.2N	148.1E	Kuriles	6.4
84339	Dec 04, 1984	07:43:23	22.6N	143.3E	Volcano Is	5.8
84345	Dec 10, 1984	10:22:05	14.8S	75.2W	Peru	5.5
85321	Nov 17, 1985	03:54:13	21.6S	179.3W	Fiji	5.2
85348	Dec 14, 1985	05:38:07	50.2N	12.4E	Germany	$3.5(m_l)$
85350	Dec 16, 1985	14:16:54	50.2N	12.4E	Germany	$3.1(m_l)$
85351	Dec 17, 1985	01:15:33	50.2N	12.4E	Germany	$3.1(m_l)$
85355	Dec 21, 1985	10:04:11	50.2N	12.4E	Germany	$3.9(m_l)$
85355	Dec 21, 1985	10:16:17	50.3N	12.3E	Germany	$4.6(m_l)$

Table III

```
CONTENTS OF GSE TAPES RECEIVED:
AUSTRIA:
WID1  1984338  4 20 12 800        2400 KBA     SPZ      SZ 20.0000000 S-13   INT8

CANADA:
WID1  1985009 10 34 15.449         401 YKA              SZ 20.0000000        INT10
WID1  1984345 10 31 34.966        3001 GAC              SZ 30.0000000        INT10
WID1  1984345 10 31 34.966        3001 GACSP            SN 30.0000000        INT10
WID1  1984345 10 31 34.966        3001 GACSP            SE 30.0000000        INT10
WID1  1984345 10 19 36.000        1801 GAC              LZ  0.5000000        INT10
WID1  1984345 10 19 36.000        1801 GAC              LN  0.5000000        INT10
WID1  1984345 10 19 36.000        1801 GAC              LE  0.5000000        INT10

ITALY:
WID1  1984342 10:28:51.880        7203 MNS     SPZ      SZ 50.0000000 S-13   INT5

JAPAN:
WID1  1984338 13 10 16 960        9000 MAT     SPZ      SZ 20.0000000 JAPAN  INT
WID1  1984338 13 10 16 960        9000 MAT     SPN      SN 20.0000000 JAPAN  INT
WID1  1984338 13 10 16 960        9000 MAT     SPE      SE 20.0000000 JAPAN  INT
WID1  1984338 13  4 58 960        8850 MAT     LPZ      LZ  1.0000000 JAPAN  INT
WID1  1984338 13  4 58 960        8850 MAT     LPN      LN  1.0000000 JAPAN  INT
WID1  1984338 13  4 58 960        8850 MAT     LPE      LE  1.0000000 JAPAN  INT
WID1  1984339 16 46  1 960        9000 MAT     SPZ      SZ 20.0000000 JAPAN  INT
WID1  1984339 16 46  1 960        9000 MAT     SPN      SN 20.0000000 JAPAN  INT
WID1  1984339 16 46  1 960        9000 MAT     SPE      SE 20.0000000 JAPAN  INT
WID1  1984339 16 40 40 960        8850 MAT     LPZ      LZ  1.0000000 JAPAN  INT
WID1  1984339 16 40 40 960        8850 MAT     LPN      LN  1.0000000 JAPAN  INT
WID1  1984339 16 40 40 960        8850 MAT     LPE      LE  1.0000000 JAPAN  INT
WID1  1984345 19 40 47 960        9000 MAT     SPZ      SZ 20.0000000 JAPAN  INT
WID1  1984345 19 40 47 960        9000 MAT     SPN      SN 20.0000000 JAPAN  INT
WID1  1984345 19 40 47 960        9000 MAT     SPE      SE 20.0000000 JAPAN  INT

SWEDEN:
WID1  1984338 04 19 20 000        4070  HFS      HFS   SZ 60.0000000 S13    INT6
WID1  1984338 04 19 20 000        4070  HFS      APP   SZ 60.0000000 S13    INT6
WID1  1984338 0  19 20 000        4070  HFS      SLL   SZ 60.0000000 S13    INT6
WID1  1984338 04 19 20 000        4070  SKI      KTB   SZ 60.0000000 S13    INT6
WID1  1984338 04 19 20 000        4070  SKI      HRN   SZ 60.0000000 S13    INT6
WID1  1984339 07 55 50 000        4070  HFS      HFS   SZ 20.0000000 S13    INT6
WID1  1984339 07 55 50 000        4070  HFS      SLL   SZ 20.0000000 S13    INT6
WID1  1984339 07 55 50 000        4070  HFS      APP   SZ 20.0000000 S13    INT6
WID1  1984339 07 55 50 000        4070  HFS      TBY   SZ 20.0000000 S13    INT6
WID1  1984338  4 20 27 927        3599 RSNY    SPZ     SZ 39.9998055 S-750  INTV
WID1  1984338  4 30 13 192        3599 RSNY    LPZ     LZ  0.9999952 KS-360 INTV
WID1  1984338  4 30 13 192        3599 RSNY    LPN     LN  0.9999952 KS-360 INTV
WID1  1984338  4 30 13 192        3599 RSNY    LPE     LE  0.9999952 KS-360 INTV
WID1  1984147 12 20 37 960        3900 MAT     SPZ     SZ 20.0000000 JAPAN  INTV
WID1  1984147 12 15 31 960        8850 MAT     LPZ     LZ  1.0000000 JAPAN  INTV
WID1  1984147 12 15 31 960        8850 MAT     LPN     LN  1.0000000 JAPAN  INTV
WID1  1984147 12 15 31 960        8850 MAT     LPE     LE  1.0000000 JAPAN  INTV
WID1  1984345 10 31 34 966        3000 GAC     SPZ     SZ 30.0000000 KS-36K INT10
WID1  1984345 10 19 36 000        1728 GAC     LPZ     LZ  0.5000000 GS-36K INT10
WID1  1984345 10 19 36 000        1800 GAC         LPN LN  0.5000000 KS-36K INT10
WID1  1984345 10 19 36 000        1800 GAC     LPE     LE  0.5000000 KS-36K INT10
WID1  1985009 10 34 15 449         400 YKA     SPZ     SZ 20.0000000 MARKII INT10
WID1  1985355 10  3 27 104        5865 CLL     SPZ     SZ 19.5300007 CIPE   INTV
WID1  1986249 23 15 12  0         3964 WMQ     SPZ     SZ 40.0000000 STS1   INTV
```


Table IV

```
FILES ACQUIRED DURING FIRST QUARTER 1987:
file name                          how acquired
----------------------------------------------------------
/a/gse/denmark/wex1test1           delivered
/a/gse/denmark/wex1test2           delivered
/a/gse/japan/84123s.mat            delivered
/a/gse/japan/84147L.MAT            delivered
/a/gse/japan/84147s.mat            delivered
/a/gse/japan/84152s.mat            delivered
/a/gse/japan/84196s.mat            delivered
/a/gse/japan/84338l.mat            delivered
/a/gse/japan/84338s.mat            delivered
/a/gse/japan/84339l.mat            delivered
/a/gse/japan/84339s.mat            delivered
/a/gse/japan/84345s.mat            delivered
/a/gse/norway/level2.sample        delivered
/a/gse/sweden/ev841203.dat         delivered
/a/gse/sweden/ev841204.swe         delivered
/a/gse/uk/test1                    delivered
/a/gse/uk/ukdec03.gse              delivered
/a/gse/uk/ukdec04.gse              delivered
/a/gse/uk/ukdec10.gse              delivered
/a/gse/usa/frgerman.data           Emailed
/a/gse/usa/gacle.tk                retrieved
/a/gse/usa/gacln.tk                retrieved
/a/gse/usa/gacsz.tk                retrieved
/a/gse/usa/ykasz.tk                retrieved
```

This table shows one potential problem with the uncontrolled exchanges which have been conducted thus far. Those files delivered by nations exist in their home directory and are given names by the delivering nation. Files E-mailed or retrieved are named by the Center staff member collecting them, but cannot be placed in the directory of the country of origin (no write permission), so they are placed in the home directory of the U.S.A. account. What should be developed is a system for naming the waveform files, as well as the designation of a waveform storage area with a directory for each nation where files can be deposited by Center staff. After a nation delivers a file, the Center should be notified by E-mail so that the file can be moved from the sending nation's home directory into the waveform storage area. For the situation where the file arrives via E-mail or is retrieved by the Center, the Center staff names the file and places it in the sending nation's directory in the waveform area.

4.1.4. Problems/Solutions

Experience has shown that the default PAD (packet assembler disassembler) settings frequently are not optimum. Nations wishing to transmit data should check for the correct PAD settings prior to each data transmission to insure optimum transfer rates. Incorrect PAD settings may increase data transmission cost by a factor of 50 or more over costs when using correct settings. Moreover, the settings for one computer may not be optimum for other computers, suggesting that records should be kept of optimum PAD settings for each transmission path.

To maintain an adequate record of data exchanges, it is important that unique identification codes be incorporated both in requests for waveforms and in the waveform data files themselves. The unique request identifier should be assigned by the nation originating a request, and the data identifier should be assigned by the nation providing waveform data. Each nation should be responsible to insure that the numbers it sends out are unique. The GSE should establish a coding system which can be used by the NDCs and IDCs to uniquely identify waveform requests and waveform transmissions. It is suggested here that the data id part of the WEX header become the file name of that data with wex prepended. Furthermore, it is suggested that the id incorporate the three-character ISO codes given in Table V. Thus, for a data package (wex, cal, wid and dat sections) provided by the U.S.A. with the data id USA001290 would have the disc-resident file name WEXUSA001290. This naming convention could also extend to physical tape labels.

It is further suggested that the GSE establish a procedure for submitting requests and a place for depositing data on each machine assigned the GSE duties. When data is deposited, a notice should be sent to the receiving nation via E-mail. It is suggested that nations' accounts and directory names also be based on the ISO three-letter codes given in Table V rather than on the full name of the nation or some ad hoc abbreviation.

Table V

NATION	ISO CODE	
	2char	3char
AUSTRALIA	AU	AUS
AUSTRIA	AT	AUT
BELGIUM	BE	BEL
BULGARIA	BG	BGR
CANADA	CA	CAN
CZECHOSLOVAKIA	CS	CSK
DENMARK	DK	DMK
EGYPT	EG	EGY
FINLAND	FI	FIN
GERMAN DEMOCRATIC REPUBLIC	DD	DDR
FEDERAL REPUBLIC OF GERMANY	DE	DEU
HUNGARY	HU	HUN
INDIA	IN	IND
INDONESIA	ID	IDN
IRAN	IR	IRN
ITALY	IT	ITA
JAPAN	JP	JPN
NETHERLANDS	NL	NLD
NEW ZEALAND	NZ	NZL
NORWAY	NO	NOR
PERU	PE	PER
ROMANIA	RO	ROM
SWEDEN	SE	SWE
UNITED KINGDOM	GB	GBR
UNITED STATES	US	USA
USSR	SU	SUN
ZAMBIA	ZM	ZMB

4.1.5.   Other Experiments

One ancillary experiment was conducted in order to determine how many station-events can be written to a single tape. A standard 2400-foot reel was used and the tape was written at 1600 bpi. A station-event is defined here as a set of four waveforms (sz and 3 lp) in standard GSE length, each preceded by its own calibration section. One station-event is written per tape file. Data from a single RSTN station was repeatably written with a complete set of four waveforms (sz, lz, ln, le) and a calibration section included in each file. Waveforms were in the standard GSE length (90 sec sz, 3600 sec lp). 288 station-events were written to the tape. Given a 50-station network, it is then reasonable to assume that one could write data for five events onto a similar tape (250 station-events). This assumes that the calibration sections from the 50 stations would be of a similar size to the one for a RSTN station. The implication here is that if all 50 stations exchanged data for 40 events a day, eight tapes a day would be required to store such data. This probably represents an upper limit since an average of 20 teleseisms were recorded each day during the GSETT and not all of these events were recorded at all stations. At the other extreme, if five events per week were selected for exchange, one tape per week would be required.

4.1.6.   New Software

Major modifications to the GSE Level II file reading program 'r2' were made during the last quarter. While no major changes to the format precipitated these changes, they are worth mentioning. r2 now has the ability to check data files for compliance with GSE rules. While the check is far from exhaustive, it will prevent random files from being processed and producing erroneous databases. Data files are tested to insure that the keywords 'WEX1', 'CAL1', 'WID1', and 'DAT1' are in place. The number of data values in the DAT section are checked to insure they equal the number of samples given in the WID section. While it is not a hard error for a file to lack a WEX or CAL section, files without WID sections are considered non-standard. A manual page has been prepared for r2, but the software has not been officially installed since it is expected that further modifications will be needed as we gain experience with the format.

Michael Tiberio
George Bullin

4-9

5. OTHER RESEARCH, STATUS OF DATABASES, SOFTWARE DEVELOPMENT

5.1. SENSITIVITY OF m_b TO EARTH ATTENUATION

5.1.1. Outline

Work is currently in progress on a study to investigate the sensitivity of m_b to earth attenuation using teleseismic recordings of presumed nuclear explosions. This is a follow-up to a previous study (Jurkevics and Romney, 1986) in which seismograms were simulated by combining a source model, near-source reflection coefficients, earth attenuation and an instrument response. The current study involves real seismograms recorded globally from presumed nuclear explosions at various sites in the U.S. and the U.S.S.R. The basic idea is to take the recorded seismograms, apply *additional* earth attenuation by a convolution operation and to then measure the change in amplitude, period and associated m_b. This approach of adding additional attenuation to recorded signals is justified by the linearity of the convolution operator with which the earth attenuation is applied. Several attenuation models are used including constant Q and frequency-dependent Q, the latter based on a linear attenuation model proposed by Minster (1978).

Short-period recordings of a total of 42 events from 12 different geographic areas are being analyzed. The events include U.S. nuclear tests and presumed U.S.S.R. weapons tests and peaceful nuclear explosions (PNEs). The source areas include the Nevada Test Sites (NTS), Amchitka Island, Degelen Mt. and Shagan River sites in East Kazakh, Novaya Zemlya, Azgir, Lake Baykal region, Kushata, and a few others. The recordings were obtained from several seismic networks including WWSSN, DWWSSN, SRO, ASRO, and RSTN. The stations were selected to provide representative global coverage, constrained by the available data in the database at the Center for Seismic Studies. Usually about 15 recordings were analyzed for each event. This note presents a few initial results and illustra⁺es the nature of the study; a more detailed account will be presented in a subsequent report.

5.1.2. Preliminary Results

Figure 1 illustrates the change in m_b for different amounts of attenuation and for three different source sizes, as represented by the three different corner frequencies. This result is for simulated seismograms and is similar to the results presented in the previously published part of the study (Jurkevics and Romney, 1986). The source model is from von Seggern and Blandford (1972), with an overshoot parameter of 0.5. A surface reflection coefficient of -0.5 at a delay of 0.25 seconds, a constant Q model, and the WWSSN short-period instrument response were used in this particular example. The m_b values in *Figure 1* have been normalized to 0.0 at $t^* = 0.0$ in order to emphasize the sensitivity, or slope, of m_b relative to t^*. *Figure 1* shows that, as expected, the m_b values from sources with lower corner frequency are less sensitive to added absorption (increased t^*) than are m_b values from high frequency sources. Further, for a given source, the
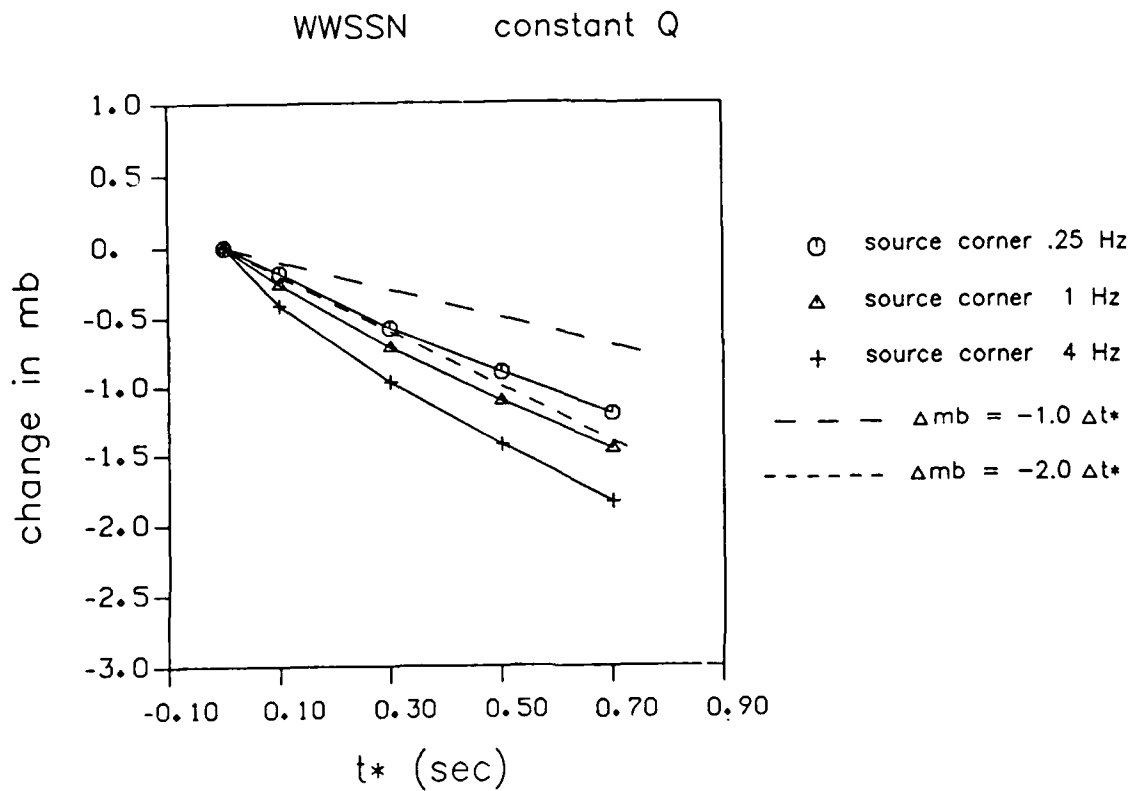
Figure 1. Sensitivity of m_b to attenuation as measured from synthetic seismograms. A von Seggern-Blandford source pulse using three different corner frequencies was tested. The instrument response is WWSSN short-period and the Q model is independent of frequency. The m_b values have been normalized at $t^* = 0$ in order to compare the slopes of the curves. The slope is a function of source corner frequency and the amount of attenuation present.

change in magnitude (Δm_b) from additional absorption (Δt^*) is a function of t^* itself. Thus, the change in magnitude resulting from transmission of P-waves through some particular absorptive layer will depend on both the spectrum of the source and on the absorption along the remainder of the path. Changes in the predominant period of P also result from changes in t^*, as noted in our earlier paper.

We apply these ideas to real seismograms from explosions as a partial test of assumptions regarding characteristics of sources at several test sites, as well as current concepts of absorption under those test sites. For instance, if we assume the NTS and Kazakh sources are identical (at a given yield) but that the absorption along the paths to a seismic station differs, then applying an additional absorption to the signals should result in changes in m_b that differ between NTS and Kazakh. Further, it should be possible to transform P waveforms from one site to model the main characteristics of those from the other by application of more attenuation.

The procedure is illustrated in *Figure 2* which shows six sets of waveforms from six different events recorded at one station; WWSSN station KTG in eastern Greenland. Each set in *Figure 2* contains three signals; the top trace is the short-period raw seismogram of the early P-wave. The two other traces in each set are the same signals with different amount of *additional* attenuation added. In this case the additional attenuation consists of a constant Q model with a t^* of 0.2 and 0.6 seconds. The three sets of seismograms along the top in *Figure 2* are from the Nevada Test Site with reported magnitudes of 6.0, 5.5 and 5.6. The three sets below are presumed tests in East Kazakh with magnitudes of 6.0, 5.9 and 5.6. The peak amplitude in nanometers is displayed adjacent to each waveform. The main effects of adding the additional attenuation are the decrease in signal amplitude and increase of low frequency energy relative to high frequency. In the analysis the m_b values were measured interactively on a SUN workstation. The so-called "c" measure was used, which is the amplitude from the first trough to the subsequent peak. While data from a single station are insufficient for drawing firm conclusions, these figures illustrate the previously reported result that NTS explosions (possibly aside from Piledriver) differ from Kazakh explosions in ways that are not explained by greater absorption under NTS.

Figure 3 shows preliminary results of analyzing actual seismograms for eight presumed PNEs located in the Azgir region of U.S.S.R. The parameter "*slope*" in the equation $\Delta m_b = slope \cdot \Delta t^*$ is plotted; this was determined by adding attenuation of $t^* = 0.2$ seconds to the seismograms. Both constant and frequency-dependent models of Q were used. The recordings were from RSTN and SRO stations with an instrument correction applied to convert to WWSSN short-period response. The station codes are shown on the graphs and the magnitudes of the events are shown below. The values plotted for each event in *Figure 2* show a considerable scatter between stations. However, the trend is to decrease the sensitivity of m_b to added t^* for increasing source size; this is qualitatively consistent with the expected decrease in corner frequency as the yield (and magnitude) increases.

Andy Jurkevics and Carl Romney

WWSSN Station KTG (Eastern Greenland)
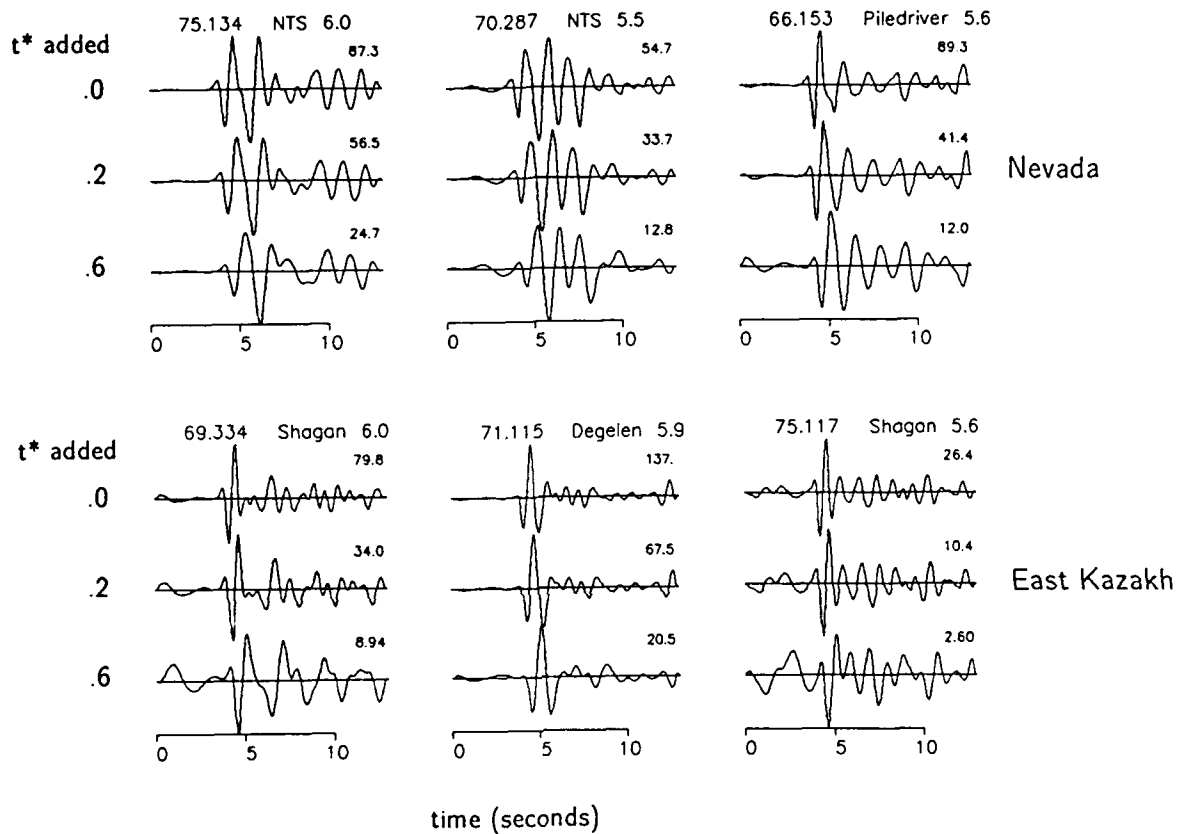
Figure 2. Attenuation is added to short-period *P*-waves from six events recorded at WWSSN station KTG. The peak amplitudes in nanometers are shown adjacent to each trace. The year.day-of-year, location, and m_b magnitude are given for each event.
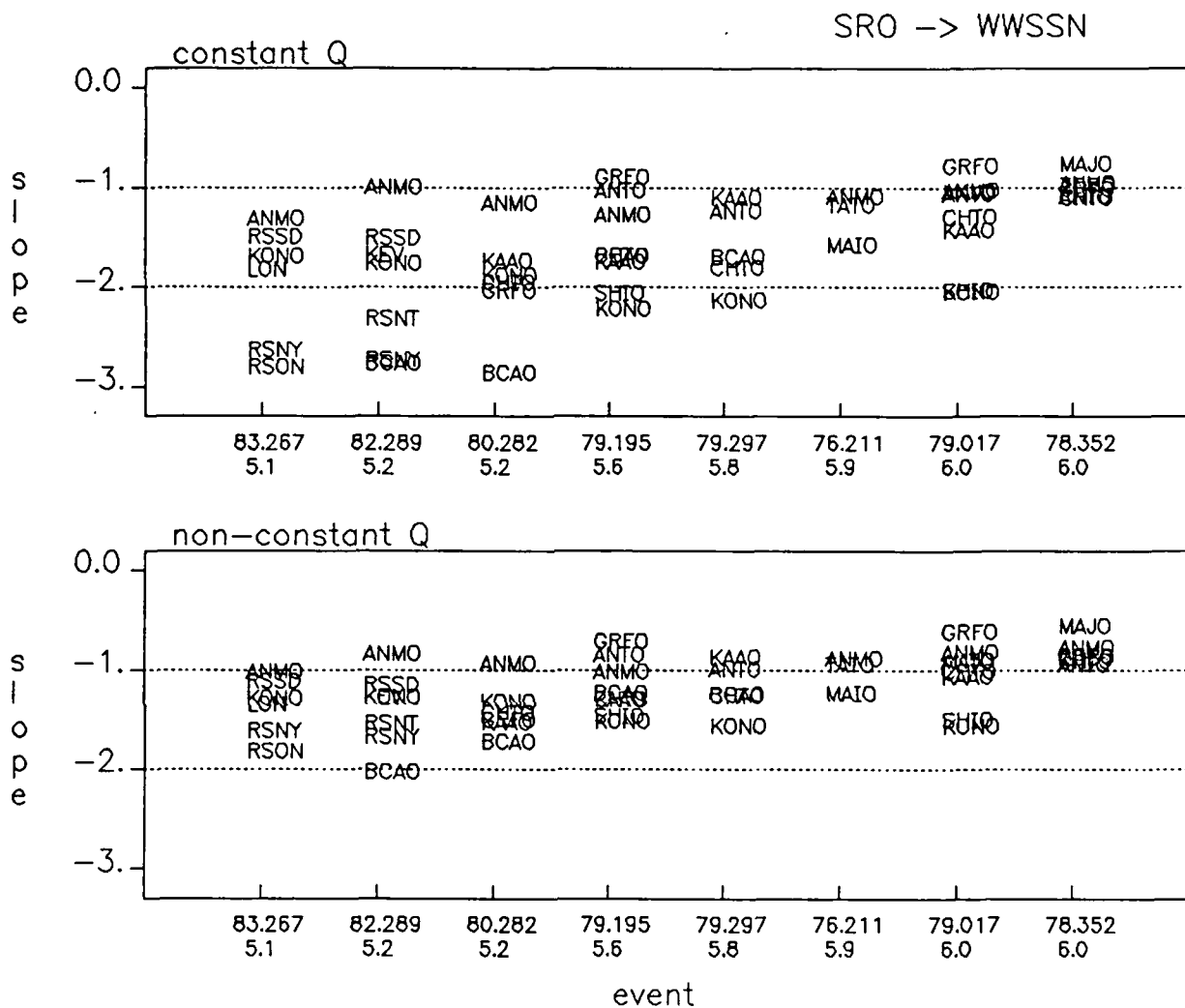
Figure 3. Observed values for "*slope*" in the relation $\Delta m_b = slope \cdot \Delta t^*$ are shown for eight presumed PNEs in the Azgir region of U.S.S.R. The recordings are from the RSTN and SRO networks. Instrument corrections were made to correct to WWSSN short-period response first. Both constant and frequency-dependent Q models were used. The year.day-of-year and m_b magnitudes are shown for each event. The m_b sensitivity is larger for the constant Q model and some dependence with magnitude is also apparent.

ACKNOWLEDGEMENTS

REFERENCES

Jurkevics, A. and C. F. Romney, 1986. "Sensitivity of m_b to Earth Attenuation," *SAIC Technical Report for the Period 1 January - 30 June 1986, Center for Seismic Studies Technical Report*, C86-07, dated July 1986.

Minster, J. B., 1978. "Transient and Impulse Responses of a One-Dimensional Linearly Attenuating Medium -- I. Analytic Results," *Geophys. Jour. R.A.S.*, Vol. 52, pp. 479.

von Seggern, D. and R. Blandford 1987. "Source Time Functions and Spectra of Underground Nuclear Explosions," *Geophys. Jour. R.A.S.*, Vol. 31, pp. 83.

5.2. BODY WAVE MAGNITUDES OF EASTERN KAZAKH EXPLOSIONS CALCULATED WITH NORESS DATA

5.2.1. Introduction

Recently the Soviet Union ended its self-imposed moratorium on nuclear weapons testing. Subsequently, three tests were conducted at its Eastern Kazakh test site, approximately 38 degrees from the NORESS array. The Center for Seismic Studies receives data from the array in real time via satellite. The NORESS data were analyzed after each test, and one of the first source parameters determined was the body wave magnitude. The m_bs calculated from the NORESS data were higher than those calculated from RSTN stations or reported by the U.S. Geological Survey's National Earthquake Information Service (NEIS). The path between Eastern Kazakh and NORESS is an efficient propagator of P-wave energy (Ringdal and Husebye, 1982). However, the m_b residuals for the three tests, +0.38, +0.74, and +1.1 m_b units, were considered large enough and different enough to warrant further review. In this study, we calculated body wave magnitudes for ten Eastern Kazakh explosions.

5.2.2. Data and Analysis

The ten explosions studied are listed in Table I. Epicentral information and m_bs are taken from NEIS's Monthly Summaries, with the exception of the 1987 events whose epicentral parameters were taken from NEIS's Quick Epicenter Determination list. Beamed P-waveforms for each event are shown in *Figure 1*, arranged in increasing order of magnitude. The waveforms show some variation with magnitude, which may reflect the increasing depth of burial. Peak-to-peak ground motions were measured from the second peak and second trough of each waveform. Some asymmetry is seen in the wave cycle of the peak-to-peak ground motion for the events on November 23, 1984, July 25, 1985, and February 26, 1987, where the first half of the cycle is of slightly lower frequency than the second half of the cycle. In these cases, the period was taken as twice the average of the cycle's half periods. The explosion on April 3, 1987 was clipped at NORESS, and the peak-to-peak amplitude was estimated by graphically extrapolating the waveforms on each side of the clipped cycle. As a check, an m_b was calculated from the unclipped intermediate-period channel and found to be the same as that estimated from the short-period beam. A "P-factor" of 3.33 (Veith and Claussen, 1972) was used for the m_b calculations. Corrected amplitudes, periods, calculated magnitudes and residuals are summarized in Table I.

Figure 2 shows a plot of the NORESS m_b values versus the NEIS worldwide average m_bs, as well as the residuals (NORESS m_b minus NEIS m_b). The open symbols refer to events at the Degelen test site, and the solid symbols refer to Shagan tests. Shagan was the site of the seven largest tests examined, whereas the smaller tests were conducted at Degelen. The mean residual for the Degelen tests is +0.21 and the mean residual for the Shagan tests is +1.00. It is also of interest to notice that for this limited dataset the residuals increase with increasing magnitude for both.

Table I

	NEIS Reported				NORESS			
Date	Lat.	Long.	m_b	Site[1]	A^2 (nm)	T (sec)	m_b	Residual
Nov. 23, 1984	49.897	78.132	4.7	D	8.2	0.4	4.64	-0.06
Dec. 16, 1984	49.957	78.862	6.1	S	2806 ·	0.6	7.00	+0.90
Apr. 25, 1985	49.924	78.969	5.9	S	1582	0.6	6.75	+0.85
Jun. 15, 1985	49.889	78.881	6.0	S	3980	0.6	7.10	+1.10
Jun. 30, 1985	49.861	78.696	6.0	S	2730	0.5	7.07	+1.07
Jul. 20, 1985	49.951	78.829	5.9	S	2492	0.6	6.91	+1.01
Jul. 25, 1985	49.894	78.150	5.0	D	47	0.5	5.30	+0.30
Feb. 26, 1987	49.787	78.122	5.2	D	89	0.5	5.58	+0.38
Mar. 12, 1987	49.958	78.834	5.6	S	609	0.6	6.34	+0.74
Apr. 3, 1987	50.59	78.67	6.1	S	6750[3]	0.6	7.3	+1.3

(1) D = Degelen, S = Shagan

(2) Peak-to-peak amplitude corrected for NORESS instrument response at period T.

(3) Estimated from clipped waveform. See text.

Ringdal (1986) showed that there is a bias between conventional network m_bs (as reported by NEIS) and maximum-likelihood m_bs, especially in the intermediate magnitude range (3.5 to 5.5). Above 5.5, the two magnitude estimates are essentially the same. Thus, the NEIS magnitudes for the Shagan explosions studied here are likely unbiased, whereas the magnitudes of the smaller Degelen shots may be overestimated. Using Ringdal's (1986) results, the NEIS magnitude for the shot on Nov. 23, 1984, should be reduced from 4.7 to 4.5, giving a residual for NORESS of +0.14. The other overestimated magnitude would be that of the July 25, 1985 shot, which would be reduced from 5.0 to 4.9, yielding a NORESS residual of +0.40. The mean residual for the Degelen shots thus becomes +0.31 versus the previous estimate of +0.21. This is, however, still considerably lower than the +1.00 mean residual for the Shagan shots.

5.2.3. Conclusion

Body wave magnitudes were calculated for ten Eastern Kazakh explosions using beams of NORESS data. The NORESS m_bs were found to be 0.2 to 0.3 units higher than network average m_bs for three explosions at Degelen, whereas at Shagan the bias was +1.00. It remains to be explained why the difference in the biases should be so large for the two areas, considering that they are only 50-70 km apart. It should also be recognized that the amplitude versus distance curve of Veith and Claussen (1972) shows a large amount of scatter. One possibility for the difference in m_b residuals may be the focusing of body waves by Degelen Mountain. As a continuation of this study, more Eastern Kazakh events will be studied using NORESS data and the results combined with the magnitude estimates presented here.

Jay J. Pulli
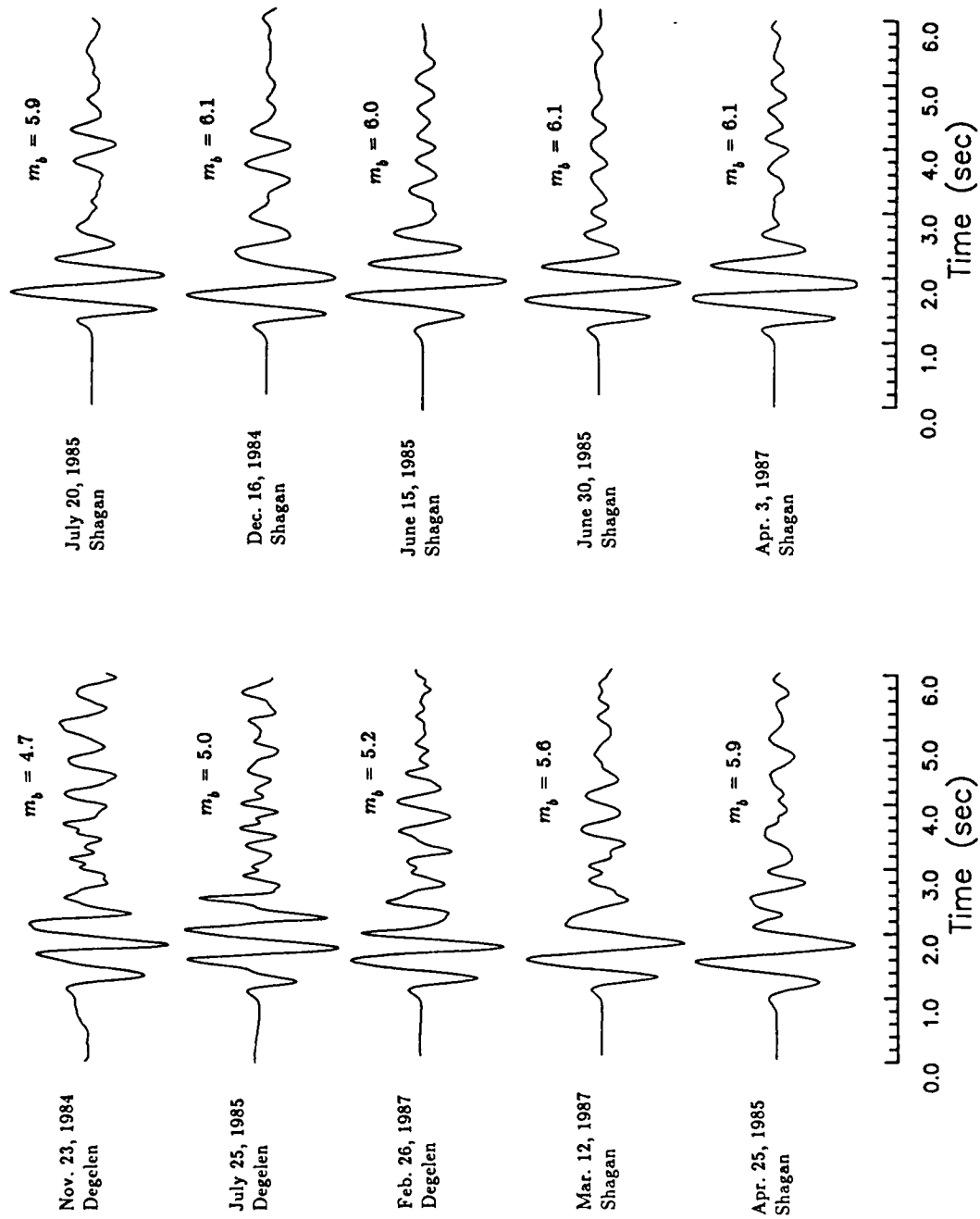
Figure 1. Beamed *P*-waveforms for ten Eastern Kazakh explosions recorded by the NORESS array. Body wave magnitudes reported by NEIS. The waveform for event 1987:093 is clipped.
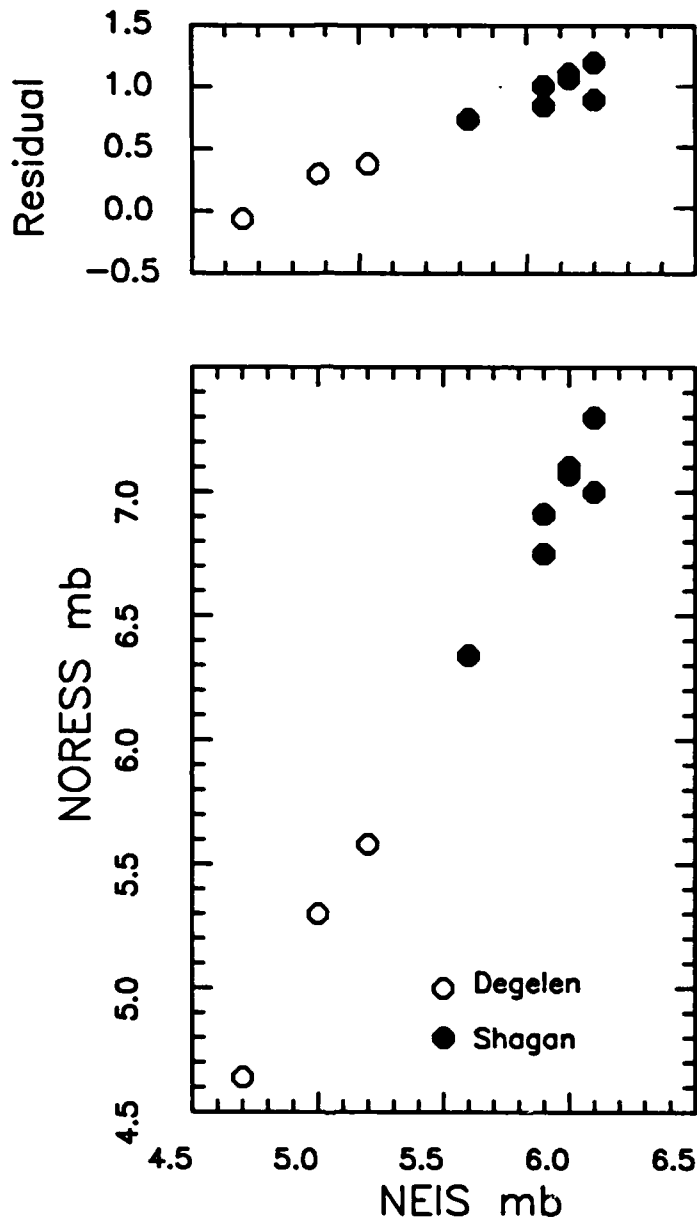
Figure 2. NORESS m_bs versus NEIS m_bs as well as residuals for the ten explosions studied.

REFERENCES

Ringdal, F., 1986. "Study of Magnitudes, Seismicity, and Earthquake Detectability using a Global Network," *Bull. Seis. Soc. Amer.*, 76: 1641-1659.

Ringdal, F. and E. Husebye, 1982. "Application of Arrays in the Detection, Location, and Identification of Seismic Events," *Bull. Seis. Soc. Amer.*, 72: S201-S224.

Veith, K. F. and G. E. Claussen, 1972. "Magnitude from Short-period P-wave Data," *Bull. Seis. Soc. Amer.*, 62: 435-452.

5.3. DETERMINATION OF AZIMUTHS OF SEISMIC EVENTS USING P AND RAYLEIGH WAVE POLARIZATION

Well determined directions of arrival of P or other seismic phases can be used to help obtain an initial approximation to the epicenter of an event, or to help associate an observed phase with the correct epicenter when two or more events occur at about the same time. The objective of this study is to determine if recently developed analysis methods can improve the direction-finding ability of three-component seismic stations, and to develop automatic methods for obtaining this information.

A polarization filter was applied to a data set extracted from the GSETT database consisting of waveforms from stations RSNY, RSON, and RSSD. Three-component short- and long-period data were obtained from 67 and 56 events, respectively, with a typical magnitude of 5.0. Input consisting of three-component seismograms (short- and long-period) are first band-pass filtered in the frequency domain. Next, in the time-domain, tapered windows are applied to all input traces where the time resolution is determined by the window length. A polarization ellipsoid is computed to isolate polarized motion. Parameters of the ellipsoid are then extracted (Jurkevics, 1985).

Table I, A and B show the deviation of the measured azimuth obtained from short-period P-waves and long-period Rayleigh waves, respectively, from the calculated azimuth to the epicenter. As noted in Table I, azimuths measured from polarization analysis of both P and Rayleigh waves are, on the average, good estimates of the direction to the epicenter. On the other hand, individual estimates may differ significantly from the calculated azimuth of the epicenter. For P-waves, RSSD has the greatest dispersion in azimuth of arrival, with a standard deviation of 79°. RSON has a much smaller dispersion. RSSD shows the largest deviation for Rayleigh waves, whereas RSNY has the smallest. Overall, standard deviations for all three stations for Rayleigh waves are quite high. Deviations may be attributed to misorientation of the instruments; failure of the theoretical wave model of the study, or may be due to inhomogenities of the earth.

Additional statistical analysis is needed to be more certain of these preliminary results. This may include dependence of accuracy on the signal-to-noise ratio, and the rectilinearity or planarity of the waveform.

Antoinette Campanella

Table I. Azimuthal Anomalies of Selected Events for RSNY, RSON and RSSD

(A - P waves)

Short-Period	Arithmetic Mean (deg.)	Standard Deviation (deg.)	Median (deg.)
All Stations (absolute values)	10.31	52.56	11.43
RSNY	-16.81	30.61	16.51
RSON	2.03	21.78	0.10
RSSD	12.10	79.29	17.67

(B - Rayleigh waves)

Long-Period	Arithmetic Mean (deg.)	Standard Deviation (deg.)	Median (deg.)
All Stations (absolute values)	7.19	62.25	7.80
RSNY	-7.76	57.66	10.19
RSON	6.63	57.56	2.08
RSSD	7.19	69.83	11.14

5.4. INVENTORY OF RUSSIAN FILM DATA AT THE CENTER

In a preliminary study of seismic signals recorded in the U.S.S.R., Ryall (1986) digitized tracings of P-waves from copies of Russian short-period recordings of several earthquakes in southeastern California. Analysis of the Soviet data, and comparison of magnitude residuals with those obtained in previous studies, led to an estimate of magnitude bias between the Nevada Test Site and a number of station sites in the U.S.S.R., including a station (SEM) at Semipalatinsk, about 100 km from the Eastern Kazakh test site.

In addition to the original data sample we now have copies on hand of long- and short-period, three-component recordings from about 40 Soviet stations, either requested by other researchers through World Data Center A or supplied as part of the International Data Exchange. This data set includes film copies of recordings of earthquakes in China, Japan, the Sea of Okhotsk, Alaska, Austria, Iran, Kamchatka, the Caucasus, Romania, and regions farther from the U.S.S.R. (*Figure 1*). Typically, data are available for a dozen or more stations for a given earthquake, and the quality of the recordings varies from very poor to very good. Station calibration constants are either marked on the records or available from the Soviet bulletins or other published reports.

These records contain direct information that can be used to estimate characteristics of body and surface wave propagation in the U.S.S.R. Studies which may be carried out with these data include the determination of receiver structure under each station from three-component data, magnitude bias versus azimuth, P- and S-wave residuals versus azimuth, and a comparison of these characteristics with the tectonics of the U.S.S.R. Crust and upper-mantle structure as well as attenuation can be estimated using the two-station transfer function method applied to surface wave paths crossing the area. If local and regional events happen to be present on the records, the data can be used to estimate local attenuation and site effects at the station. The results of such analyses can be used to increase our confidence in network evaluations by programs such as SNAP-D, and should make a significant contribution to resolving controversies stemming from differences in currently assumed propagation characteristics within the U.S.S.R.

As a first step toward creation of a database containing a representative sample of signals digitized from this record collection, we have compiled an inventory of the data on hand. Table I lists 50 events for which an adequate amount of good-quality data is available for analysis, and Table II lists 28 seismic stations which supplied most of the data. *Figure 2* shows the locations of these stations on a polar projection of the U.S.S.R. centered on latitude 66°N, longitude 90°E. Table III indicates the quality of short-period recordings available for the 50 events, with solid circles indicating "good" to "very good" quality, open circles "fair" and x's "poor" quality. Seismograms classified as "very good" had traces on which P and other phases were clearly recorded. Those rated as "good" had P-wave onsets that were clear for at least several seconds, but other parts of the record may have been unusable. "Fair" recordings typically had P onsets that were fogged or dim but probably traceable, but other parts of the signal may be poor. "Poor" signals were generally unusable as the result of under- or overexposure, intermixed traces, smudging, fogging, etc. Of a total of 457 sets of records, 41% were rated as "poor," 23%
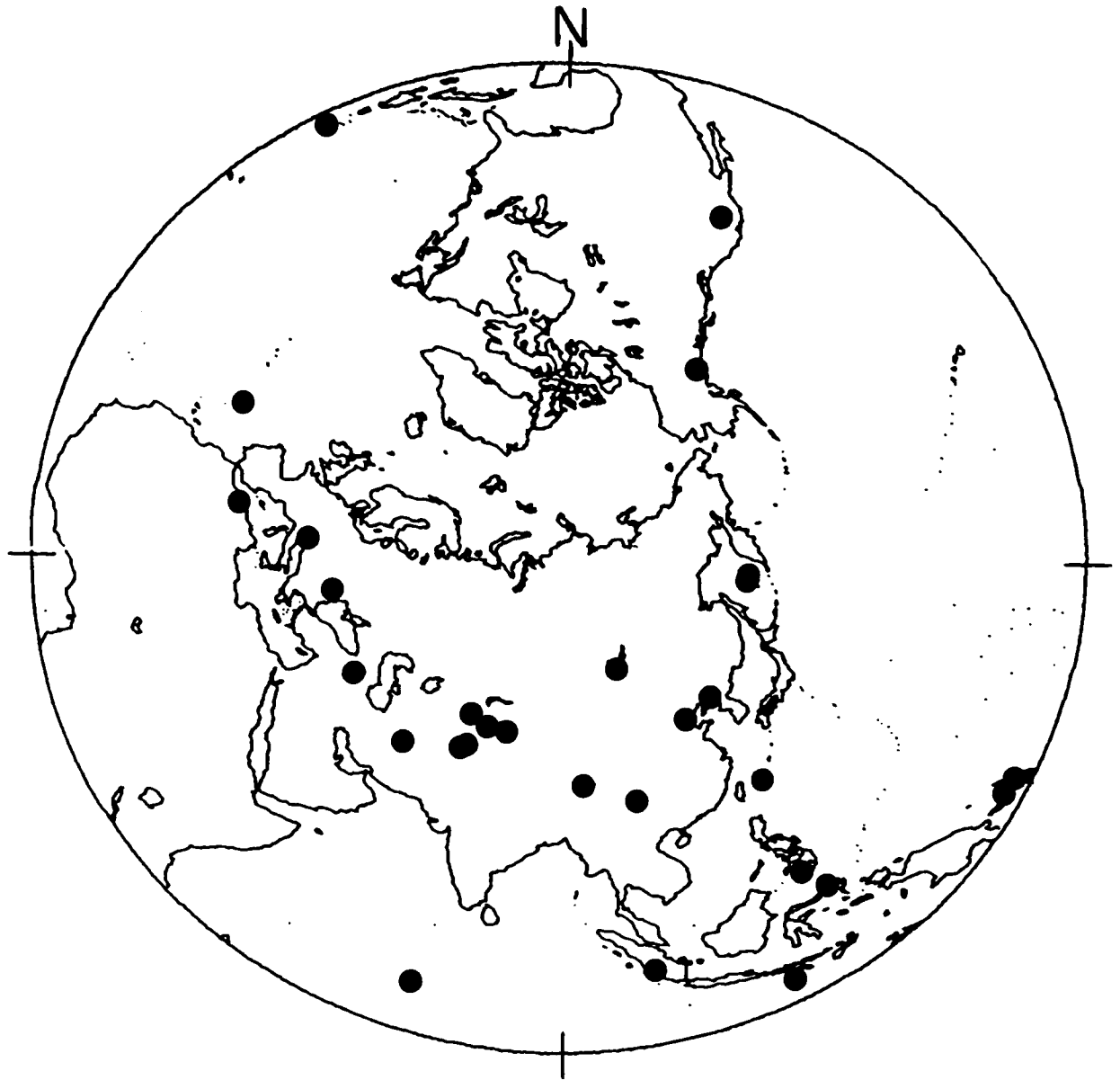
Figure 1. Events listed in Table I and Table III. Circle has radius of 90°, is centered on 83°N, 90°E.
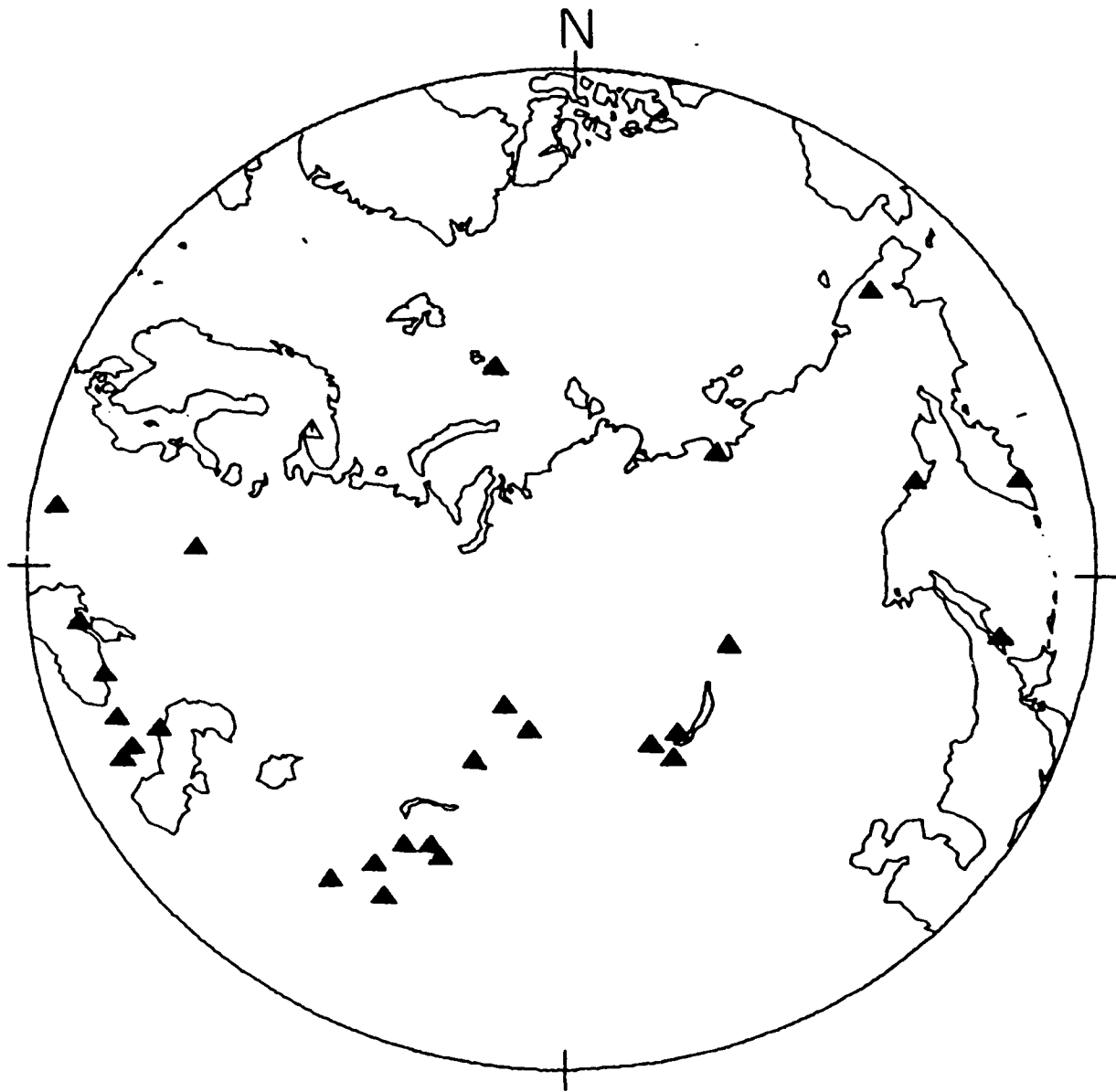
Figure 2. Location of stations listed in Table II and Table III. Circle has radius of 40°, is centered on 66° N, 90° E.

Table I. Events for which film data are available.

Event Number	Date	Time	Lat.	Long.	Depth	m_b	Remarks
01	650925	1547:56	41.52N	75.04E	12	5.2	Hindu Kush & Pamir
02	670211	0927:34	52.16N	106.48E	26	5.3	Alma Ata to Lake Baikal
03	691124	1723:19	37.16N	71.64E	113	5.8	Pamir-Hindu Kush
04	700328	0745:59	6.26S	154.62E	59	5.8	Solomon Islands
05	700328	0944:57	52.27N	105.90E	30	4.9	Lake Baikal Region
06	700830	1746:08	52.36N	151.64E	643	6.5	Sea of Okhotsk
07	700905	0752:27	52.28N	151.49E	560	5.7	Sea of Okhotsk
08	710129	2158:03	51.69N	150.97E	515	6.0	Sea of Okhotsk
09	710323	2047:16	41.42N	79.20E	14	(5.8)	Kirgiz-Sinkiang Border
10	710324	0226:14	05.28S	151.54E	69	(5.7)	New Britain Region
11	710403	0449:03	32.16N	94.99E	27	(5.6)	Tibet
12	710510	1451:45	42.85N	71.29E	14	5.6	Kirgiz
13	710615	2204:13	41.39N	79.18E	96	(5.3)	Kirgiz-Sinkiang Border
14	740510	1925:17	28.20N	104.00E	17	5.8	Szechwan Province
15	740511	0056:56	1.89N	126.47E	50	5.4	Molucca Passage
16	741003	1111:56	36.50N	70.83E	186	4.9	Hindu Kush Region
17	741003	1421:29	12.24S	77.58W	9	6.2	Near Coast of Peru
18	741008	0950:58	17.37N	61.99W	41	6.4	Leeward Islands
19	750526	0911:51	35.98N	17.56W	34	6.5	N. Madeira
20	751011	1435:15	24.91S	175.16W	11	6.4	S. Tonga
21	751226	1556:39	16.22S	172.47W	33	6.3	Samoa
22	760114	1556:33	29.48S	177.57W	29	6.4	E. Kermadec Islands
23	760204	0930:35	14.90N	90.53W	44	5.4	Guatemala
24	760506	2000:12	46.35N	13.26E	12	5.9	Austria - N.E. Italy
25	760727	1942:54	39.56N	117.87E	10	6.1	N.E. China
26	760728	0058:44	39.40N	117.76E	12	4.9	N.E. China
27	760728	0948:23	39.44N	118.03E	35	4.9	N.E. China
28	760728	1045:37	39.71N	118.37E	37	6.1	N.E. China
29	760816	1611:05	6.22N	124.10E	8	6.4	Phillipines-Mindanao
30	761124	1222:16	39.05N	44.04E	10	6.1	N.W. Iran-USSR Border
31	770304	1921:54	45.83N	26.72E	86	6.1	Romania
32	770402	0715:22	16.79S	172.02W	33	6.4	N.E. Tonga
33	770404	1906:35	02.78S	102.26E	126	5.3	S. Sumatra
34	770420	2342:53	09.94S	160.48E	33	6.1	Solomon Islands
35	770421	0424:09	10.00S	160.77E	31	6.4	Solomon Islands
36	770622	1208:33	22.91S	175.74W	69	6.3	Tonga
37	770819	0608:54	11.16S	118.41E	78	6.8	S. of Sumbawa
38	790228	2127:06	60.74N	141.55W	22	6.2	S.E. Alaska
39	791127	1710:33	34.08N	59.79E	9	6.2	Iran
40	791212	0759:04	1.62N	79.34W	28	6.2	Near Coast of Ecuador
41	800525	1633:44	37.60N	118.80W	?	6.1	Mammoth Lakes, Calif.
42	800527	1451:00	37.49N	118.78W	?	5.7	Mammoth Lakes, Calif.
43	800708	2319:19	12.49S	166.37E	29	5.9	Santa Cruz Islands
44	800717	1942:23	12.48S	166.06E	29	5.6	Santa Cruz Islands
45	801010	1225:22	36.16N	1.40E	0	6.3	Algeria
46	801108	1027:32	41.15N	124.30W	5	5.9	Near Coast of N. Calif.
47	810901	0929:31	15.08S	173.12W	20	6.5	Tonga
48	830318	0905:50	4.89S	153.57E	94	6.5	New Ireland region
49	831130	1746:00	6.85S	72.04E	10	6.5	Chagos Archipelago
50	840207	2133:20	9.96S	160.49E	4	6.5	Solomon Islands

Table II. Station Information.

Name	Code	Lat. N.	Long. E.
Andizhan	AND	40.75	72.37
Apatity	APA	67.55	33.33
Bakuriani	BKR	41.73	43.52
Bodaybo	BDB	57.85	114.18
Dushanbe	DSH	38.57	68.77
El'tsovka	ELT	53.25	86.27
Frunze	FRU	42.83	74.62
Goris	GRS	39.50	46.33
Irkutsk	IRK	52.27	104.32
Iul'tin	ILT	67.83	178.80
Kheys	KHE	80.62	58.05
Kirovabad	KRV	40.65	46.33
Magadan	MAG	59.55	150.80
Makhachkala	MAK	43.02	47.43
Mondy	MON	51.68	100.98
Murgab	MUR	38.37	73.93
Novosibirsk	NVS	55.03	82.92
Obninsk	OBN	55.17	36.45
Petropavlovsk	PET	53.02	158.65
Przheval'sk	PRZ	42.48	78.40
Semipalatinsk	SEM	50.40	80.25
Simferopol'	SIM	44.95	34.12
Sochi	SOC	43.58	39.72
Talgar	TLG	43.23	77.23
Tiksi	TIK	71.63	128.87
Uzhgorod	UZH	48.63	22.30
Yuzhno-Sakhalinsk	YSS	47.02	142.72
Zakamensk	ZAK	50.38	103.28

Table III. Quality of film data for events and stations in
Tables I and II. Solid circle—good to very good; open circle—fair; X—poor.

	01	02	03	04	05	06	07	08	09	10	11	12	13	14	15	16	17	18	19	20	21	22	23	24	25	26	27	28	29	30
ANR			X			X	X	X	○	●	X		○	X	○															
APA	X							X						X			○	○			X			X						
BKR				X	X		X	X	X	X	●	●	○								X									
BOD					○		X	X	○	X	●	○						○												
DSH					●	X	●						●	○										●						
ELT	X				X	X	X	X	●	●	X			X			○	X	X	X		●	●	●	●				○	X
FRU			○	○	X		●	X	○	X	○	X	○	X			●		X	X	○	●		●			●			
GRS				●	●	X	○	●	●	X	●	X	○					X	X	●	○	●	X		○		●	●	●	●
IRK			●	●	●	X	○	●	X	●	○	X	●	●	●			X	●	●	●	●	●		○	●	●	●	●	●
ILT				○		X	X	○	○	○	X	○	○																	
KHE											X	X	○																	
KRV									○	X	○	○								○	○	X	X		X				○	X
MAG			X		X		X	X			●	X		X	●		●	●		●	●	●	●	●			●			
MAK	●					X	X	●	●	●	●		●	X	○	●	●	X	●	●	●	●	●		●	●	●	●	●	●
MON									X	○	○	○																		
MUR	●											●																		
NVS	○	X	X				X	X	●	X	●	X		X	X	○	X	X			●	●		○	●			●		●
OBN			●					●	●	X	●	X	●	X	X	X		X		●	●	●	●	●	●	●	●		●	●
PET	X		○		X			X	X	X	○	X	X		○	○	X	○		○	○		○	●	○					○
PRZ	X	○							X	X	○	X	●	X	●	●	●	●	●	○	●	●		●	●	●	●			
SEM	X	○	○		X	X	X	X	X	X	X	X	●	●	●	●	●	●	●	●	●	●								
SIM						○	X	●	●	X	○	X	○						X	○				○						
SOC		X	X				X		X	○	O	X	X							○		○	○	●	X		●			X
TLG	X		○	○			X	X	X	X	X	X	○	X			●			○	○	○	○						●	●
TIK			●	X			X	○	●	○	●	○	●	X			●								●	●		●	●	●
UZH	X			●		X	X	X	X	○	X	X	●	X			○	X	○	○	X			X	X		X		○	X
YSS			○	X	X		X	○	●	○	X	X	●				○	●	X	X	●			X	X	●			●	●
ZAK								○	○	○	●	○	●								●						○			

Table III -- (Continued)

	31	32	33	34	35	36	37	38	39	40	41	42	43	44	45	46	47	48	49	50
ANR	O																			
APA	X		O																	
BKR			X					O					X			X	X	X	X	X
BOD											●	X								
DSH																				
ELT	X					X	●	●					●	O		O	O	X	X	X
FRU	●		O				●	●		O			●	●		O	O			
GRS			●				●	●												
IRK						X		●		●	●	●	O	●	O	●	X	X	X	X
ILT	O	●		●	●	●		●	X	●	●		●	●	●	X	●	X	O	O
KHE																				
KRU																			●	
MAG		●	X	X		O		X		X					●	●	X	X		X
MAK																				
MON																				
MUR	O							●		●			●	●		O	O	X	O	O
NVS			O	●	●			O	O	●			X	●	O	●	O	X	X	X
OBN				●				X					X	X		X	X	X	O	X
PET		●		●		X														
PRZ	X																			
SEM	X										●	●								
SIM																				
SOC		O	X	X		O	O	O		X			O	●	●	●	X	●	X	X
TLG			O	O		O	O	●	●				X	X	X	X			X	X
TIK																				
UZH		●	X	X	●	X	X	X	O	X			X	X	X		X	X	X	X
YSS		●		●	●	X	X	O	O				X	X	●	X			●	X
ZAK																				

5-20

"fair" and 36% "good" to "very good." Long-period seismograms were generally clearer than the short-period records characterized by Table III, but an inventory of long-period data has not been made.

Station SEM, because of its proximity to the Eastern Kazakh test range, is of particular interest to questions of propagation bias. That station had good quality records for seven of the 50 events, fair for another three, and poor for nine. In addition, SEM had good recordings of two events in 1965 for which the ISC Bulletin did not list locations.

The Center plans to begin hand-digitizing the best of the Soviet short-period records over the next few months, and installing the digitized traces in a special database. Progress on this effort will be reported in a Center Newsletter, which will be issued quarterly starting in June.

Alan S. Ryall, Jr.

REFERENCE

Ryall, A., 1986. "Preliminary Study of m_b Bias at Selected Soviet Seismic Stations," *Center for Seismic Studies Report*, C86-04, 36 pp.

5.5. STATUS OF NORESS AND OTHER WAVEFORM DATABASES

5.5.1. Introduction

A major goal of the Center program has been to facilitate the work of other contractors in key areas of the nuclear monitoring research program, with the Center supplying data and computer services to external users. The Center currently maintains or is preparing a sizeable number of databases. Some of these represent a complete set of information of some type and the contents are fixed, while others are undergoing development on a continual basis as new data of the same type arrive.

5.5.2. Status of Primary Databases

All Center databases are on *HUGO*, and are accessed through the *INGRES* relational database management system. *HUGO* currently allocates 1,084 Mbytes of disk space for databases, of which 945 Mbytes are filled. Status of the primary databases are given in Table I. Note in relation to the waveform databases that the term "complete" means that the Center has all data available for a particular source; "incomplete" means that additional data may be available from another agency. Some of the waveform data at the Center is in the form of waveform segments for particular events (GDSN, WAKE, SAFRICA, HDWWSSN, NORSAR), while the remaining data sets contain both continuous and segmented data.

Table I. Status of Primary Center Databases

Database	Coverage	No. Tapes	Mbytes (disk)
Parameter Data			
EVENTS	1177 BC to current	0	52.544
ISC	Nov. 1, 1978 to Dec. 31, 1978	0	19.760
ARRIVALS	May 16, 1982 to current	0	175.196
GSETT	Oct. 15, 1984 to Dec. 14, 1984	0	21.524
Waveforms-complete			
GDSN	Jan. 1, 1976 to Dec. 31, 1986	1043	256.166
RSTN	Jan. 1, 1982 to current	2975	153.024
	(dp/pdp Jan. 15, 1984 to current)	0	59.640
WAKE	Sep. 8, 1982 to Dec. 10, 1986	138	3.916
SAFRICA	Mar. 15, 1986 to Oct. 11, 1986	1	0.448
NORESS (on-line)	Oct. 29, 1986 to current	384	20.800
NORESSHF	Dec. 1, 1985 to Dec. 31, 1986	183	1.360
Waveforms-incomplete			
NORESS	Oct. 25, 1984 to Oct. 28, 1986	172	19.116
HDWWSSN	Sep. 13, 1963 to Dec. 27, 1981	4	1.752
NORSAR	Nov. 6, 1976 to Dec. 13, 1986	100	18.920

Additional sets of waveforms that are being processed for inclusion as official Center databases include Phase I and Phase II data from stations being installed and operated in Kazakhstan, U.S.S.R., in a cooperative effort by the Natural Resources Defense Council and the Soviet Academy of Sciences, and a large number of recordings of NTS explosions made under the Long Range Seismic Measurements program and the Special Data Collection Systems program. Work is also progressing on compilation of classified and unclassified versions of an **EXPLOSION** database, and on the archiving of instrument responses for all waveform data available at the Center.

5.5.3. NORESS Research Data Sets

With the DARPA/GSD program now emphasizing advanced research utilizing data from small seismic arrays, the Center has devoted considerable effort to compilation of a representative set of NORESS waveform segments for local and regional events over a range of azimuths from the NORESS array, plus waveforms for all underground nuclear explosions recorded by the array. These data are archived in three separate data sets, described below and summarized in Tables II-IV. Center users may request copies of these data sets on tar tapes, by contacting Richard Baumstark.

The Center research staff has selected recordings of 88 small earthquakes and mine blasts in Scandinavia and the western U.S.S.R. as representing the types of events recorded over a range of distance out to 15° and a range of azimuth around the array. Epicentral information for this set of waveforms, which are currently retained on disk on one of the Sun computers (*maui*), is listed in Table II together with event type taken from local station bulletins. As the table indicates, the set includes 34 earthquakes, 38 mine blasts, and 16 events for which event type was not specified in the local bulletins. Ten of the latter occurred off the southwest coast of Norway on November 20-21, 1985, and were probably earthquakes. Locations of the 88 events are shown at the top of *Figure 1*, with the circle drawn at a distance of 15° from NORESS.

Table II. Events Selected by Center Research Staff

Name	Mo-Dy	Hr:Mn:Sec	Lat	Lon	Dist	Depth	mb	Area	Type
85213	08-01	11:17:35.8	45.82	26.65	17.39	122	4.7	Romania	E
85298	10-25	12:03:47.	59.30	28.10	8.42	0	2.3	SW of Leningrad	X
85300	10-27	04:36:43	61.12	4.92	3.26	0	2.8	W Coast Norway	E
85312	11-08	14:18:54.6	58.34	6.43	3.54	0	2.4	SW Norway	X
85313	11-09	14:42:46.	57.80	7.20	3.69	0	2.1	SW Norway	X
85313b	11-09	18:20:48.	62.00	7.70	2.24	0	2.0	Norway due N?	?
85317	11-13	16:32:10.	58.30	6.40	3.54	0	1.8	SW Norway	X
85317b	11-13	12:07:48.	59.30	28.10	8.42	0	2.3	SW of Lenin	X
85324	11-20	22:10:44.2	57.61	5.67	4.35	0	2.3	SW Norway	?
85324b	11-20	22:24:38.1	57.66	5.72	4.30	0	2.2	SW Norway	?
85324c	11-20	22:57:10.0	57.64	5.62	4.35	0	2.3	SW Norway	?

Table II.   Events Selected by Center Research Staff -- (Continued)

Name	Mo-Dy	Hr:Mn:Sec	Lat	Lon	Dist	Depth	mb	Area	Type
85324d	11-20	23:10:47.5	57.66	5.35	4.43	0	2.3	SW Norway	?
85324e	11-20	23:17:28.9	57.69	5.49	4.36	0	2.3	SW Norway	?
85324f	11-20	23:23:10.0	57.50	5.62	4.45	0	2.2	SW Norway	?
85324g	11-20	23:28:23.1	57.58	5.49	4.44	0	2.2	SW Norway	?
85325	11-21	14:18:13.	59.80	8.20	1.91	0	1.4	SW Norway	?
85325b	11-21	14:48:07.	54.80	6.50	6.53	0	2.8	SW Norway	?
85325c	11-21	09:16:30.	58.37	12.36	2.41	-1	-.0	SE Norway?	?
85327	11-23	13:06:18.	59.50	25.00	6.84	0	2.1	NW Estonia	X
85331	11-27	04:53:32.8	59.73	06.71	3.08	15	2.8	W Coast Norway	E
85344	12-10	12:06:39.	59.40	28.50	8.58	0	2.2	SW of Leningrad	X
85357	12-23	02:35:08.3	60.38	01.90	4.77	15	2.3	Shetland Is	E
85358	12-24	12:37:57.	59.80	22.50	5.53	-1	1.9	S tip of Finland	?
85359	12-25	13:19:01.	58.70	26.00	7.59	0	2.6	Estonia	?
85361	12-27	12:16:08	59.40	28.50	8.58	0	2.4	SW of Leningrad	X
85365	12-31	06:57:17.	73.31	6.62	12.77	15	4.8	Greenland Sea	E
86003	01-03	14:58:41.	61.90	30.60	9.23	0	2.5	NW of Leningrad	X
86007	01-07	14:14:28.	58.34	6.43	3.54	0	2.2	SW Norway	X
86009	01-09	09:18:43.	54.70	19.50	7.40	-1	2.7	Poland	?
86017	01-17	14:11:01.	58.34	6.43	3.54	0	2.3	SW Norway	X
86019	01-19	04:59:22.	65.00	12.13	4.29	-1	3.0	N Sweden	E
86020	01-20	23:38:28.	50.19	12.37	10.58	-1	4.9	Germany	E
86021	01-21	08:55:40.	55.30	13.60	5.56	-1	2.5	S tip of Sweden?	?
86031	01-31	12:10:15.	59.30	28.10	8.42	0	3.2	SW Leningrad	X
86035	02-04	12:14:59.	59.50	26.50	7.58	0	2.8	NE Estonia	X
86035b	02-04	12:58:59.	59.4	24.00	6.67	0	2.5	NW Estonia	X
86035c	02-04	14:22:57.	59.30	24.40	6.61	0	2.6	NW Estonia	X
86036	02-05	17:53:16.	62.81	4.86	3.90	-1	4.7	Norwegian Sea	E
86037	02-06	16:29:55.	67.10	20.60	7.53	0	2.7	N Sweden	X
86037b	02-06	12:22:04.	59.30	28.10	8.42	0	2.7	SW Leningrad	X
86038b	02-07	11:00:01.	64.70	30.70	9.64	0	3.1	Karelian SSR	X
86041	02-10	12:41:46.	59.40	28.50	8.58	0	2.5	SW of Lenin	X
86045	02-14	14:13:19.	58.34	6.43	3.54	0	2.4	SW Norway	X
86045b	02-14	17:54:04.	58.34	6.43	3.54	0	2.3	SW Norway	X
86045c	02-14	12:10:21.	59.40	28.50	8.58	0	2.7	SW of Leningrad	X
86045d	02-14	16:44:08.	67.10	20.60	7.53	0	2.6	N Sweden	X
86049	02-18	10:46:16.	59.30	27.20	8.00	0	2.6	NE Estonia	X
86049b	02-18	12:45:50.	64.70	30.70	9.64	0	2.6	Karelian SSR	X
86057	02-28	02:11:44.	62.76	05.29	3.90	15	2.5	W Coast Norway	E
86062	03-03	07:26:06.	43.70	31.40	20.81	48	4.4	Black Sea	E
86064	03-06	14:16:31.	66.3	21.7	7.19	-1	.0	N Sweden?	?
86064b	03-06	12:13:19.	59.50	26.50	7.58	0	2.6	NE Estonia	X
86064c	03-06	13:02:06.	60.63	02.56	4.41	15	2.1	W Coast Norway	E

Table II.   Events Selected by Center Research Staff -- (Continued)

Name	Mo-Dy	Hr:Mn:Sec	Lat	Lon	Dist	Depth	mb	Area	Type
86067	03-08	16:21:17.	61.67	02.58	4.44	15	2.4	W Coast Norway	E
86069	03-10	12:02:09.	59.30	28.10	8.42	0	2.6	SW of Leningrad	X
86069b	03-10	04:20:04.	62.81	04.91	3.78	15	2.5	W Coast Norway	E
86070	03-11	12:02:28.	59.30	28.10	8.42	0	2.6	SW of Leningrad	X
86071	03-12	11:07:21.	59.50	26.50	7.57	0	2.5	NE Estonia	X
86071b	03-12	12:01:38.	59.40	28.50	8.58	0	2.5	SW of Leningrad	X
86078	03-19	12:06:40.	59.40	28.50	8.58	0	2.6	SW of Leningrad	X
86089	03-30	03:22:37.	61.66	04.53	3.52	15	2.2	W Coast Norway	E
86091	04-01	09:56:53.	56.42	12.10	4.35	15	3.6	Sweden	E
86094	04-04	22:42:30.	71.08	08.35	10.47	15	4.6	Norwegian Sea	E
86097	04-07	00:34:37.	61.84	04.88	3.40	15	2.3	W Coast Norway	E
86108	04-18	00:44:13.	59.22	01.42	5.30	15	2.4	Shetland Is	E
86154	06-03	14:30:04.	61.46	04.08	3.69	15	2.8	W Coast Norway	E
86155	06-04	09:06:31	61.50	30.40	9.16	0	3.3	N of Leningrad	X
86163	06-12	09:30:55.	61.50	30.40	9.16	0	3.1	N of Leningrad	X
86166	06-15	15:01:07.	61.67	03.85	3.84	15	3.0	W Coast Norway	E
86168	06-17	12:12:07.	59.4	28.5	8.58	0	2.6	SW of Leningrad	X
86169	06-18	11:05:08.	59.4	28.5	8.58	0	2.5	SW of Leningrad	X
86170	06-19	03:55:08.	59.31	06.54	2.89	0	2.4	W Coast Norway	E
86171	06-20	22:07:53.	61.47	03.92	3.77	15	2.0	W Coast Norway	E
86177	06-26	04:06:21.	61.88	05.10	3.31	15	2.4	W Coast Norway	E
86178	06-27	03:49:46.	59.28	06.76	2.81	15	2.5	W Coast Norway	E
86185	07-04	11:13:27.	59.3	28.1	8.42	0	2.6	SW of Leningrad	X
86195	07-14	13:50:32.	58.35	13.82	2.66	10	4.0	S Sweden	E
86195b	07-14	14:30:27.	61.10	29.90	8.95	0	2.9	N Finland	X
86195c	07-14	15:02:19.	69.30	34.40	12.83	0	2.9	Kola Peninsula	X
86222	08-10	05:01:04.	59.99	05.34	3.17	15	1.7	W Coast Norway	E
86228	08-16	04:24:36.	62.82	04.96	3.75	15	2.5	W Coast Norway	E
86244	09-01	22:11:26.	60.82	02.93	4.22	15	3.5	W Coast Norway	E
86273	09-30	20:02:47.	60.79	04.23	3.59	15	2.4	W Coast Norway	E
86283	10-10	19:56:31.	61.97	02.33	4.60	15	2.3	W Coast Norway	E
86299	10-26	11:45:06.	61.46	03.29	4.07	15	2.6	W Coast Norway	E
86299b	10-26	11:57:03.	61.72	03.27	4.12	15	2.6	W Coast Norway	E
86302	10-29	21:05:01.	60.81	03.04	4.17	15	2.4	W Coast Norway	E
86327	11-23	03:30:32.	73.74	09.06	13.10	10	4.7	Greenland Sea	E
86346	12-12	16:33:30.	72.96	04.80	12.55	10	4.7	Norwegian Sea	E

Table III. Events Selected by SAIC, La Jolla Group

Lat	Lon	Date	Start Time	Depth	mb
59.30	6.95	Nov. 06, 1985	14:50:50.2	10	2.3
58.00	6.60	Nov. 13, 1985	14:11:05.8	0	1.9
59.70	7.70	Nov. 21, 1985	13:16:47.2	0	1.7
58.80	4.80	Nov. 21, 1985	14:06:44.4	0	2.0
56.70	7.30	Nov. 21, 1985	15:04:34.7	0	2.3
58.30	4.80	Nov. 21, 1985	15:47:54.1	0	2.1
61.77	4.49	Nov. 30, 1985	19:05:09.4	10	3.0
60.60	10.10	Dec. 04, 1985	14:00:01.2	0	1.2
60.20	5.34	Dec. 07, 1985	14:15:32.3	10	0.0
58.80	5.70	Dec. 07, 1985	14:39:09.0	0	2.0
58.30	6.10	Dec. 31, 1985	13:36:49.6	0	2.1
58.20	6.90	Jan. 31, 1986	14:17:35.7	0	1.9
58.00	9.60	Feb. 03, 1986	15:52:59.5	0	2.8
62.40	5.80	Feb. 05, 1986	23:35:53.9	0	2.1
62.30	5.70	Feb. 06, 1986	06:20:05.4	0	1.8
62.10	6.50	Mar. 25, 1986	09:05:33.9	0	1.8
58.70	5.80	Apr. 04, 1986	13:12:43.9	0	1.9
60.30	4.90	Apr. 08, 1986	11:27:36.1	0	1.7
58.40	10.55	Apr. 09, 1986	08:16:24.9	10	2.5
58.40	10.60	Apr. 09, 1986	08:27:01.7	0	2.4
60.30	5.39	Apr. 16, 1986	11:51:11.5	10	1.8
57.90	7.40	Apr. 16, 1986	13:14:36.8	0	2.1
60.80	4.20	Apr. 28, 1986	15:52:49.9	0	2.5
58.30	4.80	Apr. 30, 1986	06:04:47.7	0	1.9
56.20	1.30	Apr. 30, 1986	06:21:05.7	0	2.7
59.31	6.88	Apr. 30, 1986	10:18:47.3	10	2.3
60.36	5.08	May 02, 1986	10:44:57.0	10	1.8
59.70	10.90	May 05, 1986	15:38:10.8	0	0.7
63.30	6.40	May 17, 1986	16:00:40.5	0	2.4
59.70	7.20	May 27, 1986	18:36:14.0	0	2.1
59.30	7.30	May 28, 1986	17:51:56.8	0	2.4
59.60	4.90	Jun. 03, 1986	11:03:23.9	0	2.1
58.50	6.50	Jun. 06, 1986	13:14:27.9	0	1.7
58.90	5.90	Jun. 23, 1986	13:12:54.0	0	1.8
59.30	7.30	Jul. 10, 1986	20:10:28.2	0	2.3
62.50	7.60	Jul. 12, 1986	13:37:46.6	0	1.9
57.70	14.30	Jul. 14, 1986	14:45:18.0	0	3.5
66.80	6.80	Jul. 15, 1986	18:45:32.9	0	3.5
59.23	7.23	Jul. 16, 1986	17:49:24.8	10	2.6

Table III. Events Selected by SAIC, La Jolla Group -- (Continued)

Lat	Lon	Date	Start Time	Depth	mb
59.30	7.40	Jul. 23, 1986	20:47:09.8	0	2.2
59.30	7.30	Jul. 29, 1986	13:13:40.5	0	2.3
59.50	7.00	Jul. 30, 1986	17:59:39.0	0	2.4
60.00	10.60	Jul. 30, 1986	22:30:13.5	0	2.1
58.30	6.70	Aug. 14, 1986	13:14:39.1	0	1.9
59.30	7.40	Aug. 14, 1986	14:39:57.3	0	2.4
59.50	7.00	Sep. 02, 1986	12:53:50.8	0	2.1
59.20	7.40	Sep. 09, 1986	17:55:57.5	0	2.4
59.20	16.00	Sep. 20, 1986	22:14:59.3	0	3.5
58.50	6.40	Oct. 01, 1986	14:15:09.6	0	1.9
57.80	7.20	Oct. 09, 1986	14:13:51.5	0	2.0
61.30	6.50	Oct. 12, 1986	14:53:15.0	0	1.5
59.60	10.80	Oct. 30, 1986	09:21:15.5	0	1.2
62.60	6.30	Nov. 01, 1986	14:55:03.8	0	2.4
58.90	12.70	Nov. 02, 1986	07:48:02.5	0	3.5
57.70	8.70	Nov. 13, 1986	08:00:29.7	0	1.8

Table IV. Nuclear Explosions Recorded at NORESS

LAT	LON	DATE	TIME	MB	GRN
73.37	54.96	Oct. 25, 1984	06:29:57.7	5.9	648
49.95	78.83	Oct. 27, 1984	01:50:10.6	6.2	329
46.86	48.10	Oct. 27, 1984	05:59:57.1	5.0	357
46.84	48.08	Oct. 27, 1984	06:04:56.7	5.0	357
37.00	-116.02	Nov. 10, 1984	16:40:00.0	4.5	41
49.90	78.13	Nov. 23, 1984	03:55:04.8	4.7	329
49.99	79.07	Dec. 02, 1984	03:19:06.3	5.8	329
49.96	78.86	Dec. 16, 1984	03:55:02.7	6.1	329
49.86	78.75	Dec. 28, 1984	03:50:10.7	6.0	329
49.88	78.82	Feb. 10, 1985	03:27:07.6	5.9	329
37.06	-116.04	Mar. 15, 1985	16:31:00.1	4.8	41
37.18	-116.09	Mar. 23, 1985	18:30:00.0	5.3	41
37.09	-116.03	Apr. 02, 1985	20:00:00.0	5.7	41
37.20	-116.21	Apr. 06, 1985	23:15:00.0	4.8	41
49.92	78.97	Apr. 25, 1985	00:57:06.5	5.9	329
-22.08	-138.90	Apr. 30, 1985	17:28:57.9	4.5	631
37.25	-116.32	May 02, 1985	15:20:00.0	5.7	41
-21.82	-139.05	May 08, 1985	20:27:58.8	5.7	631
-22.06	-138.86	Jun. 03, 1985	17:29:58.0	5.2	631
37.25	-116.49	Jun. 12, 1985	15:15:00.0	5.5	41
37.09	-116.08	Jun. 12, 1985	17:30:00.0	4.4	41
49.89	78.88	Jun. 15, 1985	00:57:00.7	6.0	329
37.12	-116.12	Jun. 26, 1985	18:03:00.0	4.3	41
49.86	78.70	Jun. 30, 1985	02:39:02.7	6.0	329
65.97	40.86	Jul. 18, 1985	21:14:57.4	5.0	724
49.95	78.83	Jul. 20, 1985	00:53:14.5	5.9	329
49.89	78.15	Jul. 25, 1985	03:11:06.5	5.0	329
37.30	-116.44	Jul. 25, 1985	14:00:00.0	5.2	41
37.00	-116.04	Aug. 17, 1985	16:25:00.0	4.6	41
37.09	-116.00	Sep. 27, 1985	14:15:00.0	4.6	41
37.21	-116.21	Oct. 09, 1985	23:20:00.0	4.2	41
37.11	-116.12	Oct. 16, 1985	21:35:00.0	4.6	41
-21.85	-138.97	Oct. 26, 1985	16:34:58.3	5.4	631
-21.86	-138.77	Nov. 24, 1985	16:00:58.5	4.7	631
-21.87	-138.93	Nov. 26, 1985	17:41:58.4	5.8	631
37.05	-116.04	Dec. 05, 1985	15:00:00.0	5.7	41
37.24	-116.47	Dec. 28, 1985	19:01:00.0	5.3	41
37.22	-116.18	Apr. 10, 198	14:08:30.1	4.9	41
37.26	-116.44	Apr. 22, 1986	14:30:00.0	5.3	41
37.10	-116.02	Jun. 05, 1986	15:04:00.0	5.3	41

Table IV. Nuclear Explosions Recorded at NORESS — (Continued)

LAT	LON	DATE	TIME	MB	GRN
37.26	-116.50	Jun. 25, 1986	20:27:45.1	5.5	41
37.28	-116.36	Jul. 17, 1986	21:00:00.0	5.7	41
37.14	-116.07	Jul. 24, 1986	15:05:00.0	4.5	41
49.81	78.17	Feb. 26, 1987	04:58:21.8	5.4	
49.93	78.79	Mar. 12, 1987	01:57:17.3	5.4	
49.90	78.81	Apr. 03, 1987	01:17:08.1	6.2	
49.85	78.69	Apr. 17, 1987	01:03:04.7	6.0	
60.78	56.22	Apr. 19, 1987	04:00:01.1	4.5	
60.67	56.30	Apr. 19, 1987	04:05:01.0	4.4	
49.75	77.99	May 06, 1987	04:02:05.6	5.4	
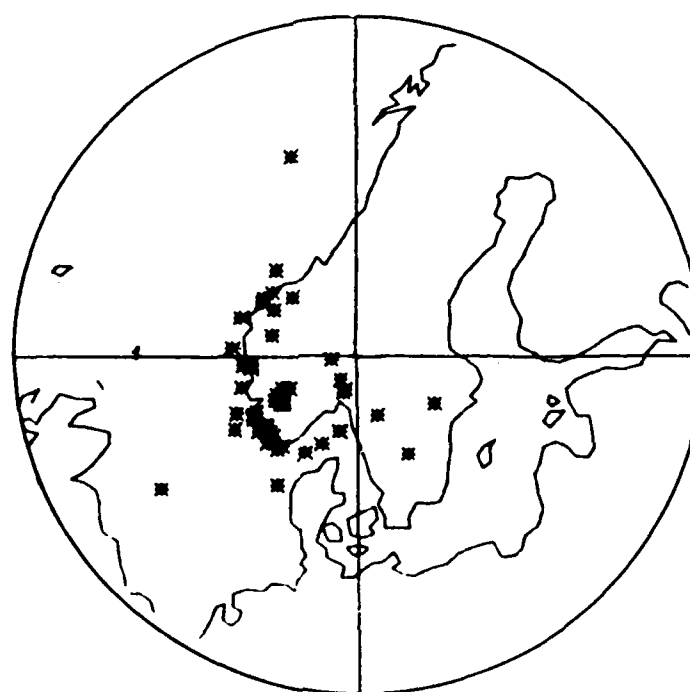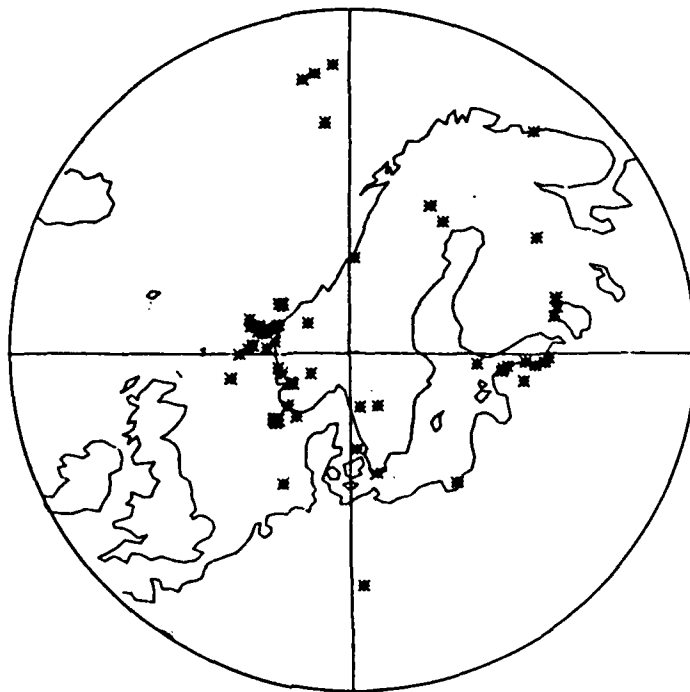
Figure 1. Top—events selected by Center research staff; bottom—events selected by SAIC, La Jolla group.

An additional set of 55 waveform segments for events in southern and western Scandinavia has been selected by the SAIC group in La Jolla. These events are listed in the Bergen, Norway, station bulletin. Selection of these events was based in part on problems identified by the NORSAR analyst -- probable error in phase association, interfering phases, incorrect identification of Lg phase—as a set of test data for development of expert system analysis tools. These events are listed in Table III and their locations are shown at the bottom of *Figure 1* (circle = 10°).

The Center now has NORESS recordings for 50 presumed underground explosions in the U.S.S.R. and on the Nevada Test Site. These events are listed in Table IV.

Richard R. Baumstark
Alan S. Ryall, Jr.

APPENDIX I

ABSTRACTS SUBMITTED FOR PRESENTATIONS AT MEETINGS

CHARACTERISTICS OF REGIONAL SEISMIC SIGNALS

Center for Seismic Studies
1300 N. 17th Street, Suite 1450
Arlington, VA 22209

ABSTRACT

The Center for Seismic Studies has been using NORESS data to test a number of seismic discrimination techniques as DARPA workstation tools. Analysis to date has included the extraction of frequency-domain spectral parameters, time-domain autoregressive parameters, and particle-motion information. The data set being used for testing includes NORESS recordings of approximately 100 events in Scandinavia and the western Soviet Union.

Particle-motion information is extracted using all the three-component sensors in the array by the covariance-matrix averaging technique (Jurkevics, 1986a,b). This information is characterized by various attributes of the polarization ellipse, separately for different frequency bands. Power-spectral estimates are obtained from the autoregressive (AR) modeling of short-period and high-frequency NORESS data, and the important information in the power spectrum is condensed into a few physical parameters. The resonance frequency and damping factor of an equivalent damped harmonic oscillator are used to characterize the spectral content of the signals (Dysart, 1986).

Characteristics of regional phases P_n, S_n and L_g have been determined using these and other techniques for blasts and earthquakes in the area of interest. For example, P_n particle motions tend to be rectilinear at the onset of the phase, and polarization is stronger at higher frequencies. For SNR > 2, P_n can be confidently distinguished from noise and L_g on the basis of rectilinearity and vertical-to-horizontal amplitude ratio. S_n particle motion is also polarized at the onset of the phase, but more difficult to identify because of lower effective SNR. The main characteristic of S_n polarization is the dominance of horizontal over vertical motion. The L_g wavetrain is generally longer and more complex than the other phases, and the most consistent L_g motions are observed around the time of the envelope maximum.

As an example of the regional discrimination problem we analyzed an m_b(NEIS) 4.6 event that occurred on 1 August 1986, during the recent Soviet nuclear testing moratorium. The event was located at 73.02° N, 56.50° E, south of Matochkin Shar strait on the eastern shore of Novaya Zemlya, U.S.S.R. Of 34 events that occurred within 200 km of this event during a 20-year period prior to 1986, all except four appear to have been underground nuclear tests and the others were probably aftershocks of one of the explosions. Analysis of the 1 August event using a number of discrimination techniques (polarization, vespagram, spectral, cepstral and autoregressive analyses) failed to eliminate the possibility that it could be a small underground nuclear test. A search for depth phases was inconclusive. GRF and NORESS signals for this event had spectral characteristics that were not unlike an m_b 4.6 presumed underground nuclear explosion in 1977, about 80 km to the northwest. This illustrates the difficulty of identifying a well-recorded seismic event, with magnitude equivalent to a tamped underground nuclear explosion of a few kilotons, located near a well-studied test site, in a stable geologic region. Far greater difficulties would be encountered in attempting to use a limited number of seismic stations to detect, locate and identify much smaller earthquakes, mine blasts and possible decoupled nuclear explosions in all parts of the U.S.S.R.

A. S. Ryall, A. Jurkevics, P. Dysart and J. J. Pulli

SELECTING SEISMOLOGICAL STATIONS OF A NETWORK
FOR GLOBAL EXPLOSION MONITORING

Center for Seismic Studies
1300 N. 17th Street, Suite 1450
Arlington, VA 22209

ABSTRACT

Assessments of seismic station networks to monitor underground nuclear explosions are usually limited to estimates of *given station networks.* That is to say, the geographical coordinates and noise characteristics of the seismological stations are given, and the capability of the network to detect a seismic event is then calculated. From the point of view of monitoring, the reverse problem is also relevant. That is to say, determine the station network that satisfies *given desirable performance criteria.* This problem is seldom addressed, partly because of its complexity and of the fact that widely accepted performance criteria are not available. In this paper we attempt to get some insight into this problem by presenting results from calculations of the capability of hypothetical networks with regard to event detection, location, and depth estimation.

Calculations for hypothetical networks with equal station spacing on a sphere suggest that about 10 stations or more provides fairly uniform detection thresholds over the sphere, although there are significant variations in areas close to where stations are located. The calculations also show that the average detection threshold is reduced somewhat faster than the logarithm of the square root of the number of stations ($\log_{10}\sqrt{n}$) and appears to be asymptotic to $\log_{10}\sqrt{n}$ for a large number of stations. Detection thresholds of stations located on shields and platforms are frequently observed to be lower than those of stations in regions of a different tectonic nature. It appears, however, impossible to achieve a reasonably uniform global coverage from networks based entirely on stations in shields and platforms areas. Comparisons are also made for hypothetical networks employing either single sensors or arrays. They suggest that a network employing small noise reducing arrays would give a slightly lower detection threshold than that of a larger network with the same total number of single sensors.

Location errors are calculated for networks with stations that have equal distance to the epicenter and are uniformly distributed around the epicenter. The calculated examples suggest the a 90 degree coverage of the source-to-station azimuth gives location errors that are only marginally larger than those for networks with complete azimuthal coverage.

The standard deviation of the estimated focal depth on the basis of first arrival times is used as a measure of the depth determination capability. This standard deviation is entirely determined by the distance range covered by detecting stations. A coverage limited to the teleseismic range 30-80 degrees gives a comparatively large standard deviation, whereas a significant improvement is obtained if observations at 15 degrees or closer can also be utilized.

The results of the calculations have been drawn upon in developing network concepts for the Group of Scientific Experts at the UN Conference on Disarmament in Geneva.

Hans Israelsson

Polarization Analysis Using an Array of Three-Component Sensors

ANDY JURKEVICS (Center for Seismic Studies, 1300 N. 17th Street, Suite 1450, Arlington, VA 22209)

A processing method is presented which computes ground-motion polarization from an array of three-component seismometers. The advantage gained by using an array is similar to the signal improvement realized in array beamforming, although the philosophy is somewhat different. The method works best when seismic noise and local earth scattering effects are uncorrelated between array sensors. In this case the variance of computed particle motions goes as $1/N$, where N is the number of seismometers in the array.

The analysis is carried out in the time domain and is very fast. An assumption is made that each frequency component has stationary polarization over several cycles duration. The data traces are bandpass filtered and time windowed into short segments. The 3x3 covariance matrix is computed at each sensor, and the covariance matrices for all sensors are averaged together. The polarization ellipsoid is then computed using an eigenvalue decomposition and various particle-motion attributes are extracted from the polarization ellipse. The frequency and time resolutions are controlled by the frequency bandwidths and time-segment lengths. The motivation for the covariance matrix averaging comes from the effectiveness of periodogram or autocorrelation ensemble averaging in power spectral estimation. The polarization analysis requires the velocities of coherent wavefronts across the array in order to time-align the data segments. However, the wavefront velocities are not required to nearly the same accuracy as needed for beamforming. Beamforming requires a time alignment between sensors of better than 1/4 cycle for constructive addition of phases. The covariance matrix averaging requires only that corresponding time segments between sensors be approximately aligned.

Examples are presented using synthetic data and seismograms recorded at NORESS, the small-aperture seismic array in Norway. The nature of scattered P coda is examined, source azimuths estimated, and different regional seismic phases are distinguished on the basis of their particle-motion signatures. This research is part of a DARPA-supported effort to develop seismic processing capabilities for Sun workstations at the Center for Seismic Studies.

Capabilities and Limitations of the GSETT
Global Seismic Station Network

HANS ISRAELSSON (Center for Seismic Studies, 1300 N 17th St.. Suite 1450. Arlington. VA 22209–3871)

In the fall of 1984 the *Ad Hoc* Group of Scientific Experts *(GSE)* at the UN Conference of Disarmament carried out a world wide Technical Test *(GSETT)* in order to study some aspects of an International Co-operative System for monitoring a nuclear test ban. More than 70 seismological stations contributed measurements over a period of two months. Data from the stations were collected and compiled at the Center for Seismic Studies in Arlington, Virginia, which acted as one of three International Data Centers during this test. The collected data constitute a unique set of measurements in that it included an extended set of parameters not ordinarily reported and many stations took unusual care in the analysis of data.

The data base at the Center in Arlington has been used to examine some seismological aspects of the GSETT station network. It is concluded that there is a significant variation in signal detection capability among the stations $(m_b \approx 4-6)$, and they also have a highly non-uniform geographical distribution. This results in a network detection capability which is strongly regionally dependent $(m_b \approx 3.6-4.6)$. The capability of the GSETT network varies not only between the Northern and the Southern Hemispheres but there is also significant lateral variation within both Hemispheres. The non-uniform geographical station distribution and variation in station detection capability also contribute to the high percentage of unassociated signal detections (about 40%). There is furthermore a significant gap between the network event detection thresholds and thresholds for carrying out other major functions. For example, the location accuracy of the GSETT network decreases significantly at $m_b \approx 5$. The capability of the GSETT network to determine surface wave magnitudes and compile other identification parameters is also significantly lower than that for event detection.

Computer experiments with a network simulation program (SNAP/D) have been carried out to study how the the GSETT network should be supplemented and upgraded so that it will perform in a more uniform and balanced manner.

Autoregressive Analysis of Regional Earthquakes and Explosions
PAUL S. DYSART (Center for Seismic Studies, Rosslyn, VA 22209)

The prediction coefficients in an autoregressive (AR) model contain amplitude and frequency information which is easily and quickly obtained without Fourier transforming the time series. By relating the prediction coefficients of the second-order AR model to a damped harmonic oscillator, this representation of seismic signals yields a set of spectral parameters which are very useful in problems of regional event discrimination, detection, and phase identification. Variations in the AR parameters with time reflect changes in the spectral character of seismic signals without the necessity of decomposing the seismogram into separate passbands. When viewed in this manner the AR parameters provide a promising means of detecting and identifying Pn, Lg, and other regional phases. An AR algorithm has been developed as part of the design of a DARPA seismic workstation. In most cases the speed of computation allows an automated spectral analysis in real time.

In this study, a resonance frequency, damping factor, power, and final prediction error (FPE) derived from the second-order AR model coeficients are used to characterize regional earthquakes and mine blasts recorded by the NORESS array in southern Norway. These parameters are computed as functions of time with frequency and time resolutions controlled by the length and overlap of a sliding window. Results indicate that the Pn resonance frequency, which estimates the dominant frequency of the spectrum, is higher for the explosions, as would be expected from events with shorter source duration. The damping factor or bandwidth is greater for explosions, as is the FPE, which is shown to be a good estimate of the signal entropy. As discriminants, both the resonance frequency and the FPE for Pn waves separate the explosions from the earthquakes, although there is an overlapping of the two populations. It appears that some correction for attenuation with distance is necessary for the more distant events. The NORESS results are consistent with the AR analysis of Eurasian events recorded at NORSAR (Tjostheim et al., 1975). A comparison of the two studies implies that the more extensive set of Eurasian events also exhibits higher frequencies and wider bandwidths for underground nuclear explosions than for earthquakes.

The Character of Regional Seismograms Recorded by the NORESS Array Implications for Event Identification and Automated Processing

JAY J PULLI
PAUL S. DYSART (both at Center for Seismic Studies Rosslyn VA 22209)

NORESS is a 25 element small aperture seismic array located in southern Norway. The array currently uses an automated processing system for the detection and location of regional events and newer systems are under development which will incorporate artificial intelligence (AI) technologies. The goal of our research is to investigate the waveform characteristics of events recorded at NORESS and determine whether or not these characteristics can be used for event identification by an AI system.

We have analyzed approximately 50 earthquakes and chemical explosions which occurred within 1500 km of NORESS. Distinct and repeatable waveform characteristics can be observed for groups of events. For example Lg waves generated by chemical explosions are band limited to less than 6 Hz whereas Lg waves generated by continental earthquakes often extend to higher frequencies. The largest waveform variations by far are for Pn waves. Pn waves generated by many explosions in the western Soviet Union arrive at NORESS as a wave packet with a sharply peaked spectrum. These spectra also show scalloping at harmonic frequencies which may be indicative of delayed or multiple shots. This is also evident in the cepstral analysis of Pn. Pn waves for earthquakes at similar distances are recorded as distinct multiple arrivals. Many explosions in Scandinavia generate Pn waves with peak frequencies in the 6 to 8 Hz range. whereas the Pn waves for earthquakes of similar magnitudes are of lower frequency.

Our experience indicates that no single rule or set of rules can be universally applied at NORESS to identify source types. Such an approach would require that path corrections be known to a high degree of accuracy. However the repeatability of waveform characteristics observed with the NORESS array suggests that a large amount of information may be accumulated in a short period of time. and event identification may be greatly aided by applying *case-based* rather than *rule-based* reasoning.

Seismic Discrimination and the 1 August 1986 Novaya Zemlya Event

A S. RYALL, A. JURKEVICS, P S. DYSART and J.J. PULLI (all at Ctr. for Seismic Studies, 1300 N. 17th St., Suite 1450, Arlington, VA 22209)

As an example of the difficulty of the discrimination problem in nuclear test ban treaty verification, we analyzed an m_b 4.6 event that occurred on 1 August 1986, during the recent Soviet nuclear testing moratorium. The event was located at 73.02°N, 56.50°E, south of Matochkin Shar strait on the eastern shore of Novaya Zemlya, USSR. Of 34 events that occurred within 200 km of this event during a 20-year period prior to 1986, all except four appear to have been underground nuclear tests and the others were probably aftershocks of one of the explosions. Analysis of the 1 August event using a number of discrimination techniques being tested as DARPA workstation tools at the Center for Seismic Studies (polarization, vespagram, spectral, cepstral and autoregressive analyses) failed to eliminate the possibility that it could be an underground nuclear test. A search for depth phases was inconclusive. Signals recorded for this event by the GRF and NORESS arrays had spectral characteristics that were not unlike an m_b 4.6 presumed underground nuclear explosion in 1977, about 80 km to the northwest.

These results illustrate the difficulty of identifying a well-recorded seismic event, with magnitude equivalent to a tamped underground nuclear explosion of a few kilotons, located near a well-studied test site, in a stable geologic region. Far greater difficulties would be encountered in attempting to use a limited number of seismic stations to detect, locate and identify much smaller earthquakes, mine blasts and possible decoupled nuclear explosions in all parts of the USSR.

END

7-87

DTIC